ISSN 2347-3487
Volume 12 Number 4
Journal of Advances in Physics

About the Transition to Turbulence Through Chaotic Distortion of Vortex Shedding

Igor V.Lebed
Zhukovsky Central Institute of Aerohydrodynamics
140180, Zhukovsky3, Moscow, Russia
e-mail: lebed-ivl@yandex.ru

Abstract

The results of direct numerical integration of the Navier-Stokes equations are evaluated against experimental data for the problem of flow around a hard sphere at rest. The evaluation is performed for both the sequence of vortex shedding regimes, replacing stable modes after the loss of stability, and the regime of turbulence replacing vortex shedding modes as Reynolds number Re increases. The evaluation demonstrates the unsuitability of classic hydrodynamics equations to interpret the phenomenon of vortex shedding. Moreover, the attainment of critical value of Re is accompanied by loss of the direction of instability development. Wrong direction of instability development results in the attainment of multiperiodic, that is, essentially chaotic, solution. Insurmountable discrepancies between calculation results and experimental data show that the chaotic deterministic solution to the Navier-Stokes equation is not suitable for interpretation of turbulence. An analogy is revealed between the sequence of modes observed in flow around a sphere as Re increases and sequence of modes in shear layer behind a cylinder with paraboloidal nose recorded while moving downstream along the contour of streamlined body. The conclusions are as follows. The turbulence of shear flow is regular unstable vortex shedding regime distorted by chaotic fluctuations. Solutions to the classic hydrodynamics equations are incapable of interpreting both regular and chaotic turbulence component. Multimoment hydrodynamics seeks for decision of these problems along the way toward an increase in the number of principle hydrodynamic values.

Keywords

Turbulence, Vortex Shedding, Multimoment Hydrodynamics

1. Introduction

Turbulent phenomena have a very strong impact on the surrounding reality. This explains the huge efforts that are aimed at the study of turbulence. Statistical methods are not sufficiently effective to predict the characteristics of the turbulent phenomena. Therefore, understanding the mechanism of origin and development of turbulence is extremely important and relevant. This understanding makes it possible to reproduce turbulent phenomena through modeling. The relative simplicity of the semi-empirical methods of calculating the turbulence encourages them to use when trying to reproduce the turbulent processes occurring in the environment and in industrial plants. However, the semi-empirical methods need to be clarified. Moreover, more rigorous calculations are required to determine their applicability ranges.

The direct numerical integration of classic hydrodynamics equations is an accurate way of modeling the unstable processes. The direct numerical integration of instability was made possible comparatively recently, about thirty years ago. However, evaluation of the results of direct numerical integration against experiment gives the possibility to do some conclusions today.

Section 2 of this paper is devoted to evaluation of the results of direct numerical integration of the Navier-Stokes equations against observed vortex shedding modes, replacing stable regimes in the problem of flow around a solid sphere at rest. In Section 3, the experimental data on transition from vortex shedding mode to turbulence in problem of flow past a sphere are analyzed. The observed turbulent regime is put in correspondence with calculated deterministic chaotic regime. The experimental data on transition to turbulence in shear layer behind an axially symmetric cylinder with paraboloidal nose are analyzed. In Section 4, the cause of the problems encountered by classic hydrodynamics is revealed. The paths of these problems decision within the frameworks of multimoment hydrodynamics are discussed.

2. Vortex shedding in problem of flow around a sphere

Analysis of the behavior of solution to the Navier-Stokes equations, after it loses stability, shows that the evolution of solution strictly follows the Landau-Hopf bifurcation scenario [1]. Namely, a solution, after it loses stability, bifurcates to a new stable position and experience either periodic or chaotic motion about it. The chaotic state is attained as a result of an infinite sequence of Hopf bifurcations. The power spectrum is discrete, approaching to continuous in the limit of infinite number of bifurcations. The chaotic state is deterministic, i.e., at a fixed initial and boundary conditions, representative point reaches the strictly defined phase space point at certain moment as many times as the calculation carried out.

ISSN 2347-3487
Volume 12 Number 4
Journal of Advances in Physics

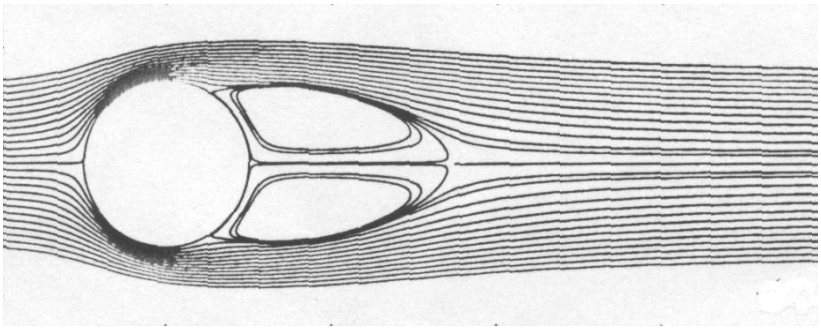

Figure 1. Stable stationary flow $\mathbf{U}_0^{cal}(\mathbf{x})$, $\mathrm{Re} < \mathrm{Re}^*$. Figure 1 was drawn using the calculation results obtained in [3].

The direct numerical integration of the Navier–Stokes equations in the problem of flow around a solid sphere at rest was performed by various numerical methods. Nevertheless, the results of all these numerical experiments were absolutely identical (see review [2]). In this problem with time independent boundary conditions, calculation finds two stationary stable velocity distributions, $\mathbf{U}_0^{cal}(\mathbf{x})$ and $\mathbf{U}_1^{cal}(\mathbf{x})$, and a non-stationary stable one-periodic velocity distribution, $\mathbf{U}_2^{cal}(t,\mathbf{x})$. Apart from the $\mathbf{U}_0^{cal}(\mathbf{x})$, $\mathbf{U}_1^{cal}(\mathbf{x})$, and $\mathbf{U}_2^{cal}(t,\mathbf{x})$ solutions, the Navier–Stokes equations only have a multiperiodic, that is, essentially chaotic, solution $\mathbf{U}_3^{cal}(t,\mathbf{x})$.

Figure 1 draws the flow picture represented by streamlines of the $\mathbf{U}_0^{cal}(\mathbf{x})$ stationary stable solution. Figure 1 shows an axially symmetric toroidal recirculating zone(vortex) in the near wake behind the sphere, which originates a single rectilinear thread in the far wake.

The stability of the $\mathbf{U}_0^{cal}(\mathbf{x})$ solution with respect to small perturbations $\delta\mathbf{U}_0^{cal}(t,\mathbf{x})$ was studied in [4]. The linearized Navier-Stokes equations for $\delta\mathbf{U}_0^{cal}(t,\mathbf{x})$ were solved in cylindrical coordinates. Hydrodynamic value perturbations were expanded in a Fourier series in time t and the azimuthal angle φ,

$$\delta\mathbf{U}_0^{cal}(t,r,z,\varphi) = \sum_{m=-\infty}^{m=\infty} \delta\mathbf{U}_0^{(\mathrm{m})cal}(t,r,z,\varphi) = \sum_{m=-\infty}^{m=\infty} \delta\mathbf{U}_0^{(\mathrm{m})cal}(r,z)\exp(\sigma_{\mathrm{m}}^0 t + im\varphi) \qquad (2.1)$$

In Equation (2.1), $i = \sqrt{(-1)}$; m is the azimuthal mode number; σ_m^0 is the rate of growth (decay) of mode perturbations; and r, z and φ are the cylindrical $\mathbf{x}$ vector coordinates. The direction of the z axis of the system of coordinates coincides with the velocity vector of the free-stream flow.

The eigenvalues of the rate σ_m^0 of changes in mode perturbations corresponding to the azimuthal wave number $m = 1$ are shown in Fig. 2. The eigenvalues move from left to right as Re increases. Two leaders are ahead of the well-defined front of eigenvalues. After the attainment of Re^*, the first leader with zero imaginary part ($\mathrm{Im}(\sigma_1^0) = 0$) intersects the axis of ordinates. According to (2.1), small $\delta\mathbf{U}_0^{(1)cal}(t,r,z,\varphi)$ perturbations, which are damped at $\mathrm{Re} < \mathrm{Re}^*$, begin to grow at $\mathrm{Re} > \mathrm{Re}^*$. It is shown in [4] that the mode with $m = 1$ predominates in expansion (2.1); that is, this is the mode that most strongly influences the stability of the $\mathbf{U}_0^{cal}(\mathbf{x})$ solution. It follows that the $\mathbf{U}_0^{cal}(\mathbf{x})$ solution, which is stable at $\mathrm{Re} < \mathrm{Re}^*$, loses stability upon the attainment of Re^*. As distinct from the approach used in [4], a non-stationary approach was applied in [3],[5]. In accordance with [3],[5], an increase in $\delta\mathbf{U}_0^{(1)cal}(t,r,z,\varphi)$ effects the saturation of a new stable non-axisymmetric solution to the Navier-Stokes equations, $\mathbf{U}_1^{cal}(\mathbf{x})$. The transition from $\mathbf{U}_0^{cal}(\mathbf{x})$ to $\mathbf{U}_1^{cal}(\mathbf{x})$ proceeds during the time interval $\Delta t_{0,1}$. The $\mathbf{U}_{0,1}^{cal}(t,\mathbf{x},\mathrm{Re}^*)$ time-dependent solution ($0 \le t \le \Delta t_{0,1}$) describes this transition (regular bifurcation).

ISSN 2347-3487
Volume 12 Number 4
Journal of Advances in Physics

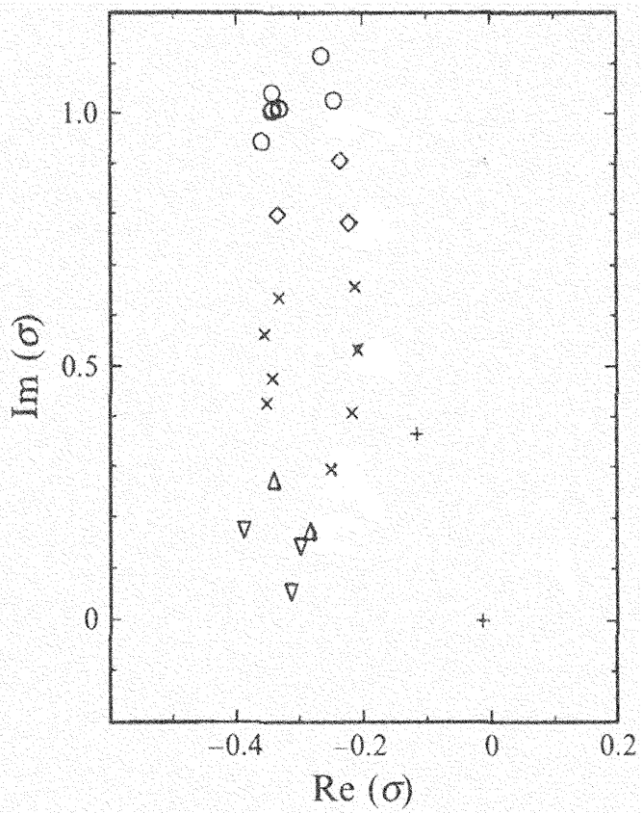

Figure 2. Eigenvalues of the rate of mode perturbation changes σ_m^0 corresponding to the predominant mode $m=1$. Figure 2 was drawn using the calculation results obtained in [4].

In accordance with the flow pattern represented by streamlines of the $\mathbf{U}_1^{cal}(\mathbf{x})$ non-axisymmetric stationary solutions [3], the upper and lower half of the near wake behind a sphere (Fig. 1) are weakly asymmetrical. Each of the near wake halves originates its own rectilinear thread in the far wake. According to the linear calculation of [4], Re^* = 210, the calculation of [3] gives Re^* = 211, the calculation of [5] gives Re^* = 212. The Reynolds number is calculated from the sphere diameter.

The second leader (Fig. 2) with a nonzero imaginary part ($\mathrm{Im}(\sigma_1^0)\neq 0$) intersects the axis of ordinates after the attainment of $\mathrm{Re}^{**}>\mathrm{Re}^*$. It follows that the $\mathbf{U}_1^{cal}(\mathbf{x})$ solution stable at $\mathrm{Re}<\mathrm{Re}^{**}$ loses stability. Increasing perturbations result in the saturation of the $\mathbf{U}_2^{cal}(t,\mathbf{x})$ stable one-period limiting cycle [3],[5]. The transition from $\mathbf{U}_1^{cal}(\mathbf{x})$ to $\mathbf{U}_2^{cal}(t,\mathbf{x})$ proceeds during the time interval $\Delta t_{1,2}$. The $\mathbf{U}_{1,2}^{cal}(t,\mathbf{x},\mathrm{Re}^{**})$ time-dependent solution ($0\le t\le\Delta t_{1,2}$) describes this transition (Hopf bifurcation).

The flow picture shown in Fig. 3 gives an idea of the total period of recirculating zone oscillations in the $\mathbf{U}_2^{cal}(t,\mathbf{x})$ wake behind a sphere [4]. The vortex structure of the lower recirculating zone half (Fig. 3) plays a very passive role during the period of oscillations T. It weakly moves and weakly changes in size. Conversely, the vortex structure in the upper half exhibits considerable activity. Its center periodically moves from the surface of the sphere to the periphery of the recirculating zone and the size of this structure periodically changes. Periodic restructuring that occurs in the near wake causes wave motion in the far wake. According to the linear calculation of [4], Re^{**}=277.5, the calculation of [3] gives $270\le\mathrm{Re}^{**}\le 280$, the calculation of [5] gives $270\le\mathrm{Re}^{**}\le 285$.

ISSN 2347-3487
Volume 12 Number 4
Journal of Advances in Physics

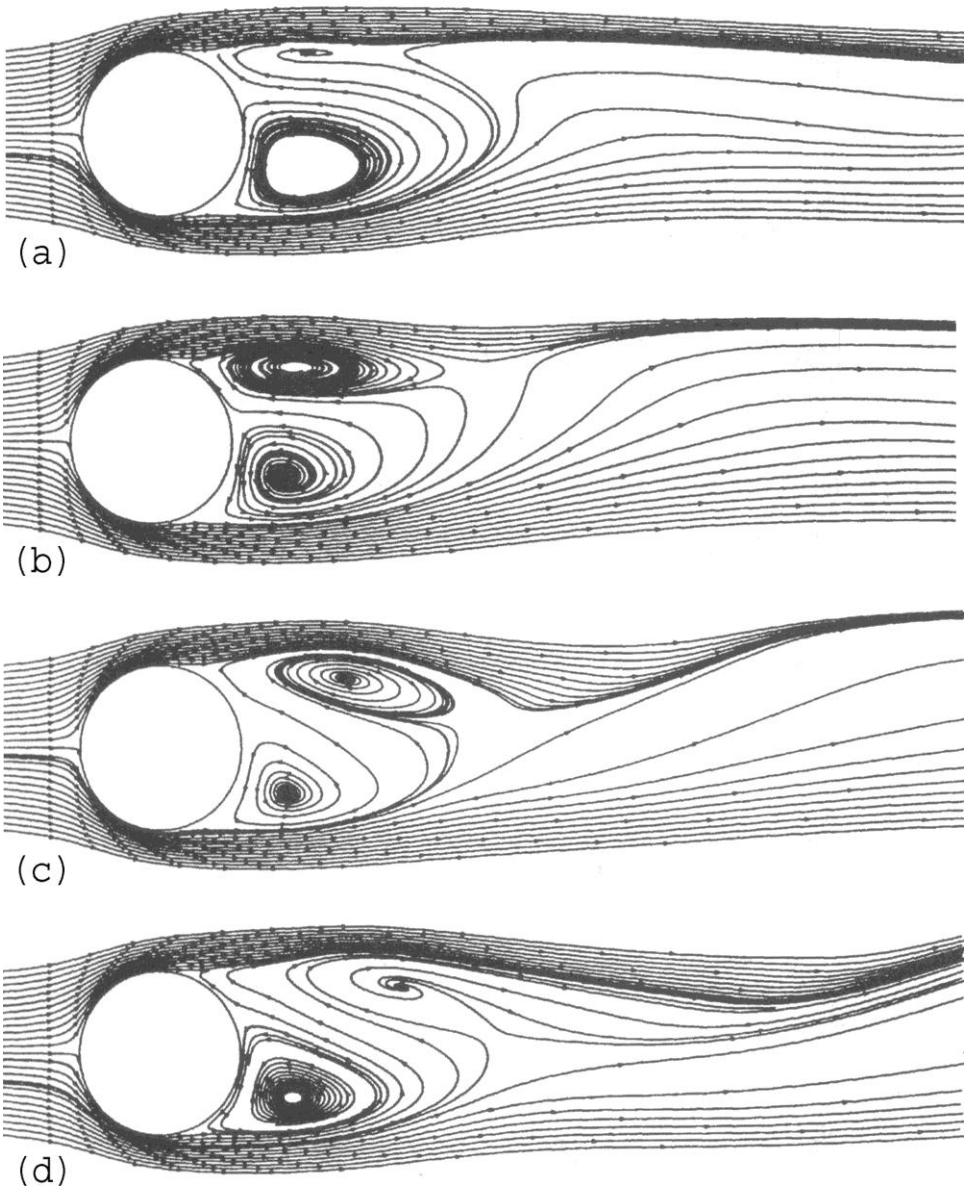

Figure 3. Stable limiting cycle $\mathbf{U}_2^{cal}(t,\mathbf{x})$, $\mathrm{Re}^{**} < \mathrm{Re} < \mathrm{Re}^{***}$, $\mathrm{Re} = 300$. Streamline picture for every quarter of the period of oscillations T. Figure 3 was drawn using the calculation results obtained in [3].

The front of eigenvalues (Fig. 2) has two well-defined lines. The first eigenvalue of the first front line reaches the axis of ordinates at $\mathrm{Re}^{***} > \mathrm{Re}^{**}$. After the passage of Re^{***}, the $\mathbf{U}_2^{cal}(t,\mathbf{x})$ limiting cycle loses stability. As Re increases, each of the front eigenvalues intersects the axis of ordinates. When the last of eigenvalues of the second front line intersects the axis of ordinates, solution finds a new stable position $\mathbf{U}_3^{cal}(t,\mathbf{x})$ about which multiperiodic, that is, essentially chaotic, motion occurs [5]. The time-dependent solution $\mathbf{U}_{2,3}^{cal}(t,\mathbf{x},\mathrm{Re}^{***},\mathrm{Re}^{****})$, $0 \le t \le \Delta t_{2,3}$, describes the transition from $\mathbf{U}_2^{cal}(t,\mathbf{x})$ to $\mathbf{U}_3^{cal}(t,\mathbf{x})$. According to the calculation of [5], Re^{***} =300.

In accordance with the Landau-Hopf scenario, the system finds inself in a stable state at each instant and at each Re. The exception is made for short periods of time, $\Delta t_{0,1}$ at $\mathrm{Re} = \mathrm{Re}^{*}$, $\Delta t_{1,2}$ at $\mathrm{Re} = \mathrm{Re}^{**}$, and $\Delta t_{2,3}$ at $\Delta\mathrm{Re} = \mathrm{Re}^{****} - \mathrm{Re}^{***}$. During these intervals, the flow experiences the restructuring which is completed by saturation of a new stable position.

ISSN 2347-3487
Volume 12 Number 4
Journal of Advances in Physics

It may be suggested that the field of the σ_1^1 eigenvalues of the $\delta\mathbf{U}_1^{(1)cal}(t,r,z,\varphi)$ mode perturbation of the $\mathbf{U}_1^{cal}(\mathbf{x})$ stationary non-axisymmetric solution should not be qualitatively different from the field of the σ_1^0 eigenvalues of the $\delta\mathbf{U}_0^{(1)cal}(t,r,z,\varphi)$ mode perturbation of the $\mathbf{U}_0^{cal}(\mathbf{x})$ stationary axisymmetric solution at $\mathrm{Re} > \mathrm{Re}^{*}$. And at $\mathrm{Re} > \mathrm{Re}^{**}$, the field of the σ_1^2 eigenvalues of the $\delta\mathbf{U}_2^{(1)cal}(t,r,z,\varphi)$ mode perturbation of the $\mathbf{U}_2^{cal}(t,\mathbf{x})$ stationary nonaxisymmetric solution should not be qualitatively different from the field of the σ_1^0 eigenvalues of the $\delta\mathbf{U}_0^{(1)cal}(t,r,z,\varphi)$ mode perturbation of the $\mathbf{U}_0^{cal}(\mathbf{x})$ stationary axisymmetric solution. Calculations [3],[5] substantiated this suggestion.

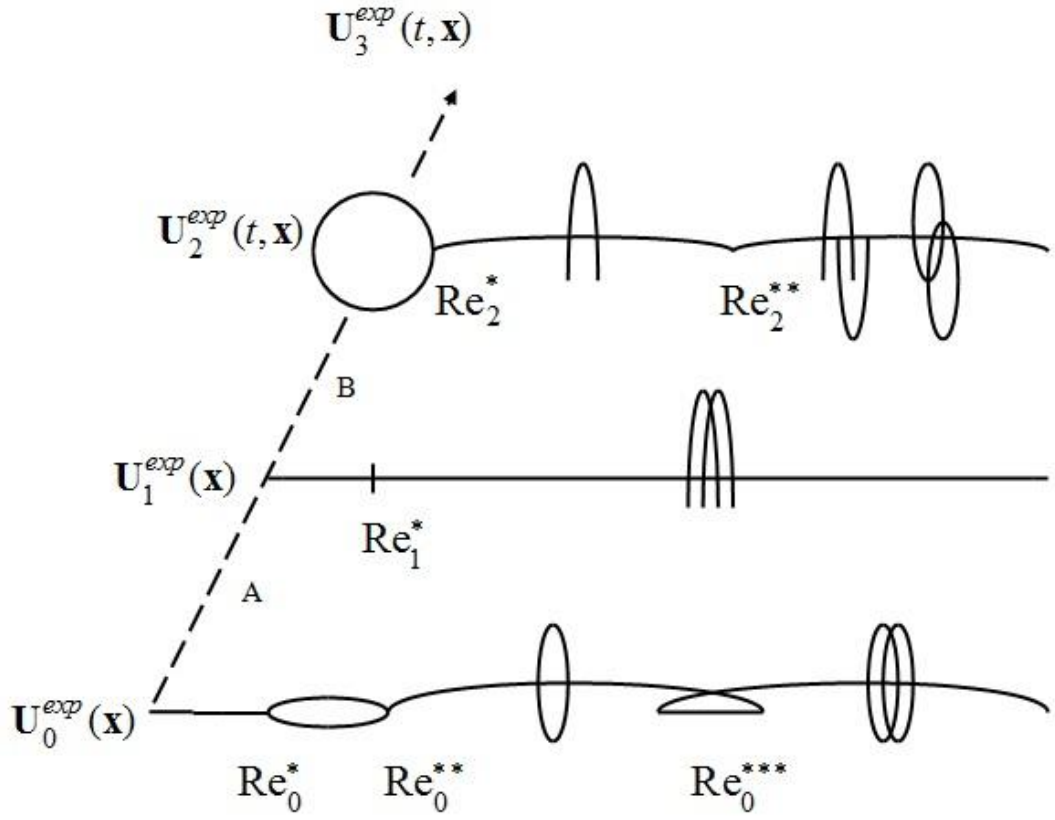

Figure 4. Three stable medium states originating three turbulence development directions for flow past a sphere. The lower branch corresponds to the evolution of stationary axisymmetric flow $\mathbf{U}_0^{exp}(\mathbf{x})$: $\mathrm{Re} < \mathrm{Re}_0^{*} - \mathbf{U}_0^{exp}(t,\mathbf{x})$; $\mathrm{Re}_0^{*} < \mathrm{Re} < \mathrm{Re}_0^{**}$, periodic pulsations of the axisymmetric recirculating zone in the wake behind a sphere $\mathbf{V}_0^{exp}(t,\mathbf{x})$; $\mathrm{Re}_0^{**} < \mathrm{Re} < \mathrm{Re}_0^{***}$, vortex ring shedding along a spiral path $\mathbf{W}_0^{exp}(t,\mathbf{x})$; and $\mathrm{Re} > \mathrm{Re}_0^{***}$, helicoidal vortex sheet $\mathbf{Q}_0^{exp}(t,\mathbf{x})$. The middle branch corresponds to the evolution of stable steady non-axisymmetric flow $\mathbf{U}_1^{exp}(\mathbf{x})$: $\mathrm{Re}_1 < \mathrm{Re} < \mathrm{Re}_1^{*} - \mathbf{U}_1^{exp}(\mathbf{x})$; $\mathrm{Re} > \mathrm{Re}_1^{*}$, periodic horseshoe-shaped vortex loop shedding along a rectilinear path $\mathbf{V}_1^{exp}(t,\mathbf{x})$. The upper branch corresponds to the evolution of a stable central-type state $\mathbf{U}_2^{exp}(t,\mathbf{x})$: $\mathrm{Re}_2 < \mathrm{Re} < \mathrm{Re}_2^{*} - \mathbf{U}_2^{exp}(t,\mathbf{x})$; $\mathrm{Re}_2^{*} < \mathrm{Re} < \mathrm{Re}_2^{**}$, periodic horseshoe-shaped vortex loop shedding along one of the double undulated thread branches $\mathbf{V}_2^{exp}(t,\mathbf{x})$; and $\mathrm{Re} > \mathrm{Re}_2^{**}$, periodic vortex loop shedding along both double undulated thread branches $\mathbf{W}_2^{exp}(t,\mathbf{x})$, or periodic vortex ring shedding $\mathbf{Q}_2^{exp}(t,\mathbf{x})$.

That is, the field of eigenvalues exhibits exceedingly conservative behaviour. The replacement of the $\mathbf{U}_0^{cal}(\mathbf{x})$ solution with the $\mathbf{U}_1^{cal}(\mathbf{x})$ solution in eigenvalue field calculations does not cause changes in the direction of evolution at $\mathrm{Re} > \mathrm{Re}^{*}$, and the replacement of the $\mathbf{U}_0^{cal}(\mathbf{x})$ solution with the $\mathbf{U}_2^{cal}(t,\mathbf{x})$ solution does not cause changes in the direction of evolution at $\mathrm{Re} > \mathrm{Re}^{**}$. That is, the results of linear calculation shown in Fig. 2 have neither qualitative no significant quantitative differences from the corresponding results in exact calculations [3],[5] within the whole range of Reynolds number Re. Namely, within the frameworks of linear calculation, the $\mathbf{U}_0^{cal}(\mathbf{x})$ basic stationary solution correctly reproduces both the direction of instability development and the critical values of Re calculated strictly in [3],[5].

Linear analysis allows us to count all the medium stable states. Linear calculation allows us to find such characteristic features of the medium stable states as the wave number (m) and the frequency $\mathrm{Im}(\sigma_m^0)$. However, the possibilities of linear analysis are limited. Linear calculations are not able to give more detailed information about the structure and parameters of new saturated stable flow.

In the problem of flow around a solid sphere at rest, experiment records two stable medium states represented by the $\mathbf{U}_0^{exp}(\mathbf{x})$ and $\mathbf{U}_1^{exp}(\mathbf{x})$ velocity distributions, and a stable state of the central type with the $\mathbf{U}_2^{exp}(t,\mathbf{x})$ velocity distribution. The $\mathbf{U}_0^{cal}(\mathbf{x})$ axisymmetric stationary solution (Fig. 1) satisfactorily reproduces the $\mathbf{U}_0^{exp}(\mathbf{x})$ observed axially symmetric recirculating zone in the near wake behind a sphere, which originates a single rectilinear thread in the far wake. The $\mathbf{U}_1^{cal}(\mathbf{x})$ non-axisymmetric stationary solution satisfactory reproduce the $\mathbf{U}_1^{exp}(\mathbf{x})$ observed two weakly asymmetric halves in the near wake behind a sphere with double rectilinear thread in the far wake. The $\mathbf{U}_2^{cal}(t,\mathbf{x})$ limiting cycle (Fig. 3) satisfactorily reproduces the $\mathbf{U}_2^{exp}(t,\mathbf{x})$ periodic restructuring of recirculating zone in the near wake behind a sphere, which causes wave motion in the far wake.

According to the analysis of [2], the direction of turbulence development is directly determined by level of medium fluctuations (disturbances). If the level of medium fluctuations does not differ or slightly differs from the level of thermodynamic fluctuations, turbulence develops in a quite specific direction. If the level of fluctuations far exceeds the level of thermodynamic fluctuations, the system selects a qualitatively different direction of turbulence development. The level of medium fluctuations is determined by both the turbulence coefficient of running flow k and various factors that distort the flow (see, review [2]).

Thermodynamic fluctuation level can only be achived in experiments in which a sphere is dragged horizontally through an unperturbed medium at a strictly controlled constant velocity. Then, toroidal recirculating zone in the near wake behind a sphere $\mathbf{U}_0^{exp}(\mathbf{x})$ (Fig. 1) begins to pulsate periodically after the attainment of a certain critical Reynolds number Re_0^{*}. The recirculating zone remains toroidal during pulsations, and its forefront is firmly fixed on the sphere. The $\mathbf{V}_0^{exp}(t,\mathbf{x})$ pulsating flow remains axisymmetric, lower branch in Fig. 4. The pulsations become increasingly well defined as Re increases, and their amplitude grows. After the passage of Re_0^{**}, the periphery of the recirculating zone begins to be periodically shed from its core and moves downstream. The shed vortex structure has the shape of a ring. Vortex rings depart from a sphere downstream and move along the spiral path $\mathbf{W}_0^{exp}(t,\mathbf{x})$ (Fig. 5a). The attainment of Re_0^{***} is accompanied by a change in the regime of vortex shedding from a sphere. At $\mathrm{Re} > \mathrm{Re}_0^{***}$, vortex rings penetrate into each other and form the $\mathbf{Q}_0^{exp}(t,\mathbf{x})$ continuous spiral sheet in the wake behind a sphere (Fig. 5b).

The development of turbulence proceeds in a different direction in experiments where liquid drop or solid body settles in medium under the action of gravitation. In these experiments, the level of fluctuations greatly exceeds the thermodynamic level due to body vibration caused by the flow circulation in the wake. Then, the attainment of a certain Reynolds number Re_1 is accompanied by a rearrangement of the $\mathbf{U}_0^{exp}(\mathbf{x})$ stationary axisymmetric flow. Namely, flow $\mathbf{U}_0^{exp}(\mathbf{x})$ transforms into stationary stable nonaxisymmetric flow $\mathbf{U}_1^{exp}(\mathbf{x})$ (Fig. 4).

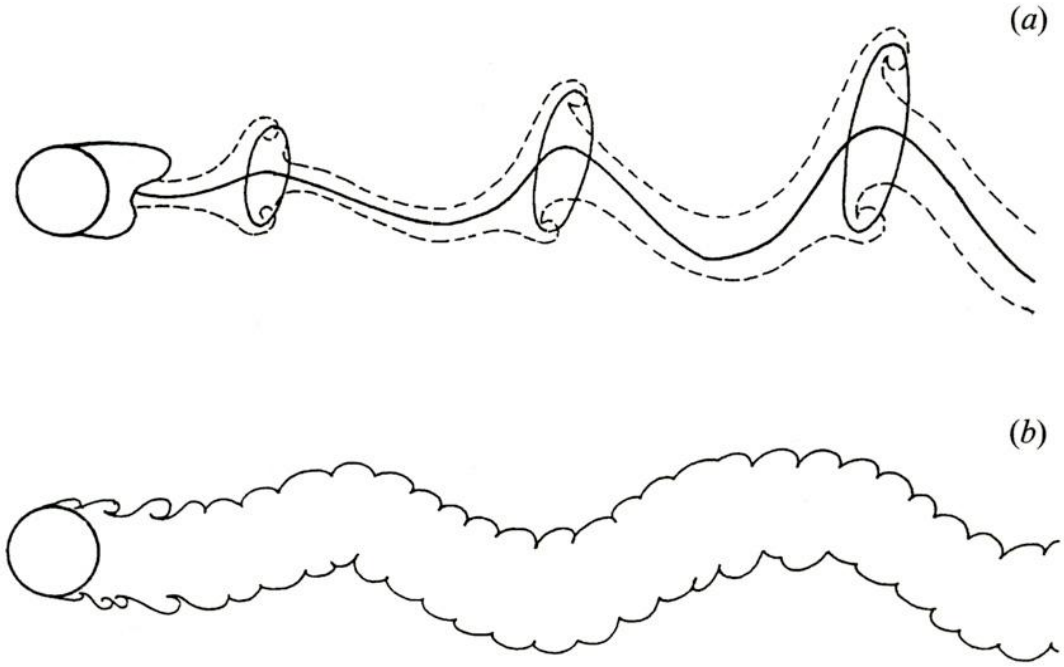

Figure 5. a) vortex ring shedding along a spiral path $\mathbf{W}_0^{exp}(t,\mathbf{x})$, $\mathrm{Re}_0^{**} < \mathrm{Re} < \mathrm{Re}_0^{***}$; b) helicoidal vortex sheet $\mathbf{Q}_0^{exp}(t,\mathbf{x})$, $\mathrm{Re} > \mathrm{Re}_0^{***}$. Figure 5 was drawn using the experimental data from [6].

At the instant when the $\mathbf{U}_1^{exp}(\mathbf{x})$ flow loses stability, experimental evidence also suggests two variants of instability development. Experiment [7] performed in water tunnel registers periodic street of horseshoe-shaped vortex loops. Vortex loops oriented in the same direction move from a sphere downstream along a rectilinear path, the middle branch in Fig. 4. Experiments performed in air tunnels have a significantly higher level of fluctuation in comparison with the fluctuation level of experiments performed in water tunnels. Experiments carried out in air tunnels find another direction of turbulence development. The attainment of a certain Reynolds number Re_2 is accompanied by a rearrangement of the $\mathbf{U}_1^{exp}(\mathbf{x})$ stationary nonaxisymmetric flow. Namely, flow $\mathbf{U}_1^{exp}(\mathbf{x})$ transforms into nonstationary stable nonaxisymmetric state of central type $\mathbf{U}_2^{exp}(t,\mathbf{x})$ (Fig. 4).

After the attainment of a certain critical value of Reynolds number Re_2^*, the $\mathbf{U}_2^{exp}(t,\mathbf{x})$ flow becomes unstable. Horseshoe-shaped vortex loops are detached periodically from the recirculating zone core and rush downstream along one of the double undulated thread branches $\mathbf{V}_2^{exp}(t,\mathbf{x})$, Fig.6a. The attainment of the next critical value of the Reynolds number $\mathrm{Re}_2^{**} > \mathrm{Re}_2^*$ is accompanied by the appearance of the next vortex shedding mode $\mathbf{W}_2^{exp}(t,\mathbf{x})$ in the wake behind a sphere, Fig.6b. At $\mathrm{Re} > \mathrm{Re}_2^{**}$, horseshoe-shaped loops shed at two symmetry-coupled points move along two different double undulated thread branches. In addition, these vortex loops have diametrically opposite orientations. According to [9], two vortex shedding modes existed at $\mathrm{Re} > \mathrm{Re}_2^{**}$. Apart from the $\mathbf{W}_2^{exp}(t,\mathbf{x})$ mode discussed above, the $\mathbf{Q}_2^{exp}(t,\mathbf{x})$ regime was observed. In the $\mathbf{W}_2^{exp}(t,\mathbf{x})$ mode, horseshoe-shaped vortex loops are shed, whereas the $\mathbf{Q}_2^{exp}(t,\mathbf{x})$ mode is characterized by vortex ring shedding. The selection of one of the two development variants, $\mathbf{W}_2^{exp}(t,\mathbf{x})$ or $\mathbf{Q}_2^{exp}(t,\mathbf{x})$, was a matter of chance in each separate experiment [9]. This direction of development is represented by the upper branch in Fig. 4.

ISSN 2347-3487
Volume 12 Number 4
Journal of Advances in Physics

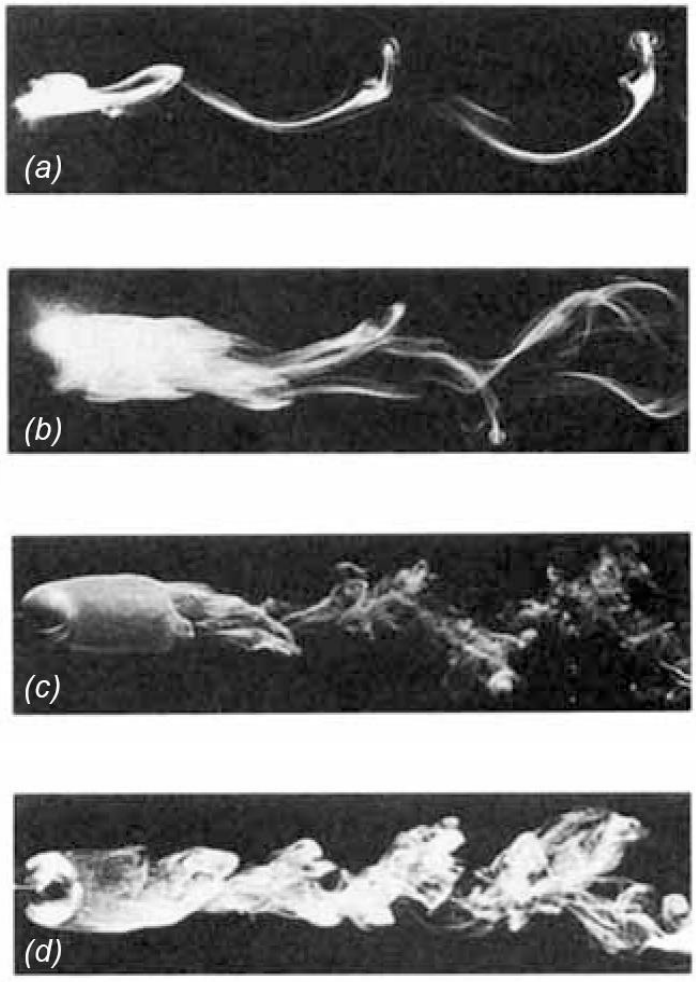

Figure 6. a) periodic horseshoe-shaped vortex loop shedding along one of the double undulated thread branches $\mathbf{V}_2^{exp}(t,\mathbf{x})$ in uniform flow, $\mathrm{Re} > \mathrm{Re}_2^*$, $\mathrm{Re} = 350$; b) periodic vortex loop shedding along both double undulated thread branches $\mathbf{W}_2^{exp}(t,\mathbf{x})$ in uniform flow, $\mathrm{Re} > \mathrm{Re}_2^{**}$, $\mathrm{Re} = 650$; c) the $\mathbf{W}_2^{exp}(t,\mathbf{x})$ mode in uniform flow, $\mathrm{Re} > \mathrm{Re}_2^{**}$, $\mathrm{Re} = 1350$; d) the $\mathbf{V}_2^{exp}(t,\mathbf{x})$ mode in shear flow, $\mathrm{Re} > \mathrm{Re}_2^*$, $\mathrm{Re} = 1444$. Figure 6 was drawn using the experimental data from [8].

In accordance with the interpretation of existing experimental data of [2], strong fluctuations inevitably cause the system to pass from the $\mathbf{U}_0^{exp}(\mathbf{x})$ state to some point A (Fig. 4), from which the system passes to the $\mathbf{U}_1^{exp}(\mathbf{x})$ state. At $\mathrm{Re} > \mathrm{Re}_0^*$, the system cannot return from point A to the $\mathbf{U}_0^{exp}(\mathbf{x})$ state because the $\mathbf{U}_0^{exp}(\mathbf{x})$ state is unstable at $\mathrm{Re} > \mathrm{Re}_0^*$. The absence of strong fluctuations allows us to track the growth of small perturbations of the $\mathbf{U}_0^{exp}(\mathbf{x})$ stationary state, that is, record the behavior in time of the $\mathbf{U}_0^{exp}(\mathbf{x})$ state itself, which loses stability at $\mathrm{Re} > \mathrm{Re}_0^*$ (the lower branch in Fig. 4). The strictly uniform profile of the flow running against a body corresponds to the boundary conditions of experiments, which guide the system along the lower branch in Fig. 4. It follows that the boundary conditions of these axperiments correlate with the boundary conditions of modeling. The boundary conditions of experiments where a liquid drop or hard body settles in a medium under the action of gravity, generally speaking, do not correlate with the boundary conditions of modeling. However, according to the calculation, after attainment of Re^*, the $\mathbf{U}_0^{cal}(\mathbf{x})$ solution, after it loses stability, bifurcates to the $\mathbf{U}_1^{cal}(\mathbf{x})$ stationary solution. The transition from $\mathbf{U}_0^{cal}(\mathbf{x})$ to $\mathbf{U}_1^{cal}(\mathbf{x})$ is at variance with the interpretation of experimental data.

A high level of medium fluctuations causes the transition of the system from the $\mathbf{U}_1^{exp}(\mathbf{x})$ state to a certain point B (Fig. 4), from which the system passes to the $\mathbf{U}_2^{exp}(t,\mathbf{x})$ state. At $\mathrm{Re} > \mathrm{Re}_1^*$, the system cannot return from point B to the $\mathbf{U}_1^{exp}(\mathbf{x})$ state because the $\mathbf{U}_1^{exp}(\mathbf{x})$ state is unstable at $\mathrm{Re} > \mathrm{Re}_1^*$. If the level of fluctuations is insufficient for the system to jump into point B, experiment records the behavior in time of the $\mathbf{U}_1^{exp}(\mathbf{x})$ state itself, which loses stability at $\mathrm{Re} > \mathrm{Re}_1^*$ (the middle branch in Fig. 4). According to the calculation, after attainment of Re^{**}, the $\mathbf{U}_1^{cal}(\mathbf{x})$ solution, after it loses stability, bifurcates to $\mathbf{U}_2^{cal}(t,\mathbf{x})$ limiting cycle. However, calculation does not take into account the fluctuation jump. It follows that the transition from $\mathbf{U}_1^{cal}(\mathbf{x})$ to $\mathbf{U}_2^{cal}(t,\mathbf{x})$ is at variance with the interpretation of experimental data.

Thus, experiment records six vortex shedding modes $\mathbf{W}_0^{exp}(t,\mathbf{x})$, $\mathbf{Q}_0^{exp}(t,\mathbf{x})$, $\mathbf{V}_1^{exp}(t,\mathbf{x})$, $\mathbf{V}_2^{exp}(t,\mathbf{x})$, $\mathbf{W}_2^{exp}(t,\mathbf{x})$, and $\mathbf{Q}_2^{exp}(t,\mathbf{x})$, and one pulsation mode $\mathbf{V}_0^{exp}(t,\mathbf{x})$. Each of six vortex shedding modes is characterized by its own characteristic features intrinsic in it. Different experiments record different vortex shedding modes. However, irrespective of the experiment, periodic vortex shedding is an obligatory, well defined, and fairly prolonged along Reynolds numbers mode of the development of a turbulent process. The flow picture shown in Fig. 7 gives an idea of the appearance of vortex street. Vortex loop or vortex ring is periodically shed from the core of the non-axisymmetric recirculating zone $\mathbf{U}_2^{cal}(t,\mathbf{x})$ and rushes downstream along the undulated path $\mathbf{V}_2^{exp}(t,\mathbf{x})$, or $\mathbf{W}_2^{exp}(t,\mathbf{x})$, or $\mathbf{Q}_2^{exp}(t,\mathbf{x})$ (the upper branch in Fig. 4). Similarly, vortex loop is periodically shed from the core of the non-axisymmetric recirculating zone $\mathbf{U}_1^{exp}(\mathbf{x})$ and rushes downstream along the straight path $\mathbf{V}_1^{exp}(t,\mathbf{x})$ (the middle branch in Fig. 4). Vortex ring is periodically shed from the core of the axially symmetric, pulsating, recirculating zone $\mathbf{V}_0^{exp}(t,\mathbf{x})$ and rushes downstream along a spiral path $\mathbf{W}_0^{exp}(t,\mathbf{x})$ or $\mathbf{Q}_0^{exp}(t,\mathbf{x})$ (the lower branch in Fig. 4).

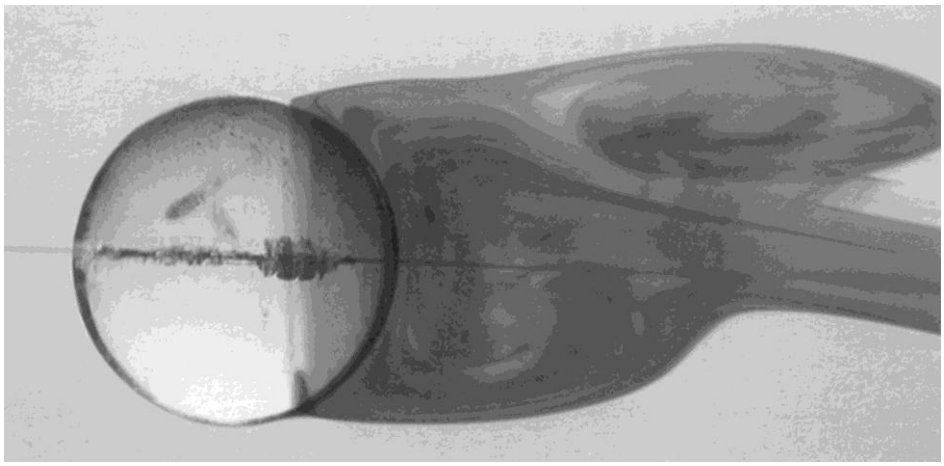

Figure 7. The detachment of the periphery of the recirculating zone originating a horseshoe-shaped vortex loop moving downstream, regime $\mathbf{V}_2^{exp}(t,\mathbf{x})$, $\mathrm{Re}_2^* < \mathrm{Re} < \mathrm{Re}_2^{**}$, $\mathrm{Re} = 300$. Figure 7 was drawn using the experimental data from [3].

The $\mathbf{U}_2^{cal}(t,\mathbf{x})$ stable limiting cycle is likely the only possibility of establishing correlation between the observed vortex shedding modes and the results of numerical integration. Indeed, the $\mathbf{U}_0^{cal}(\mathbf{x})$ and $\mathbf{U}_1^{cal}(\mathbf{x})$ solutions are stationary. The $\mathbf{U}_{0,1}^{cal}(t,\mathbf{x},\mathrm{Re}^*)$, $\mathbf{U}_{1,2}^{cal}(t,\mathbf{x},\mathrm{Re}^{**})$, and $\mathbf{U}_{2,3}^{cal}(t,\mathbf{x},\mathrm{Re}^{***},\mathrm{Re}^{****})$ non-periodic solutions are limited in time. The $\mathbf{U}_3^{cal}(t,\mathbf{x})$ mode following after the $\mathbf{U}_2^{cal}(t,\mathbf{x})$ monoperiodic limiting cycle is multiperiodic, that is, chaotic in essence. Correlation of $\mathbf{U}_3^{cal}(t,\mathbf{x})$ with the observed strictly periodic vortex loops street is hardly possible.

It follows that the $\mathbf{U}_2^{cal}(t,\mathbf{x})$ monoperiodic limiting cycle must reproduce all the observed regular nonstationary periodic modes. The idea of bringing the $\mathbf{U}_2^{cal}(t,\mathbf{x})$ stable solution to interpret the six observed vortex shedding modes and the pulsation mode in wide range of Reynolds number values initially seems to have no prospects. Moreover, this idea is not able to resolve the encountered discrepancies when evaluating the results of calculation against experiment. Indeed, at each $\mathrm{Re} > \mathrm{Re}_0^*$, the $\mathbf{U}_2^{cal}(t,\mathbf{x})$ solution should simultaneously correspond to several non-stationary modes. For instance, at some $\mathrm{Re} > \mathrm{Re}_0^{***}$ value, experiment records four different vortex shedding modes, $\mathbf{Q}_0^{exp}(t,\mathbf{x})$ on the lower branch, $\mathbf{V}_1^{exp}(t,\mathbf{x})$ on the middle branch, and $\mathbf{W}_2^{exp}(t,\mathbf{x})$ and $\mathbf{Q}_2^{exp}(t,\mathbf{x})$ on the upper branch (Fig. 4). One solution, namely, $\mathbf{U}_2^{cal}(t,\mathbf{x})$ cannot however simultaneously correspond to four qualitatively different vortex shedding modes. Moreover, only three of six modes, $\mathbf{W}_0^{exp}(t,\mathbf{x})$, $\mathbf{V}_1^{exp}(t,\mathbf{x})$, and $\mathbf{V}_2^{exp}(t,\mathbf{x})$ are monoperiodic, whereas the $\mathbf{Q}_0^{exp}(t,\mathbf{x})$, $\mathbf{W}_2^{exp}(t,\mathbf{x})$, and $\mathbf{Q}_2^{exp}(t,\mathbf{x})$ modes are two-periodic. Clearly, the $\mathbf{U}_2^{cal}(t,\mathbf{x})$ monoperiodic solution can by no means be put in correspondence to two-periodic modes.

In [3],[5], the attempt was executed to attract the $\mathbf{U}_2^{cal}(t,\mathbf{x})$ stable one-period limiting cycle to interpret the $\mathbf{V}_2^{exp}(t,\mathbf{x})$ vortex shedding mode at $\mathrm{Re}^{***} > \mathrm{Re} > \mathrm{Re}^{**}$. Let us consider the flow picture represented by streamlines in Fig. 3. After the appearance in the upper half of the wake behind a sphere (Fig. 3a), the size of the vortex structure becomes substantial at the surface of the sphere (Fig. 3b). Subsequently, the structure moves toward the periphery of the recirculating zone, which is accompanied by its continuous dissipation (Fig. 3c). Lastly, it fully disappears at the periphery of the recirculating zone (Fig. 3d). Because of the absence of the detachment of the recirculating zone periphery in Fig. 3, there is no vortex loop street in the wake behind a sphere. This picture is qualitatively different from the observed full period of oscillation of the recirculating zone [3]. As in calculations, the experimental vortex structure engendered begins to expand and move downstream. After reaching the periphery of the recirculating zone, this vortex structure, however, acquires a maximum size rather than dissipates as predicted by calculations. At the end of the period, the vortex localized at the periphery of the recirculating zone separates from this zone. The separation of the shed vortex from the recirculating zone is very clearly shown in Fig. 7. The periphery of the recirculating zone, which is periodically shed from the recirculating zone, rushes downstream and forms a vortex loops street (Fig. 6a). Therefore, the $\mathbf{U}_2^{cal}(t,\mathbf{x})$ stable solution is incapable of reproducing the $\mathbf{V}_2^{exp}(t,\mathbf{x})$ vortex shedding mode at $\mathrm{Re}^{***} > \mathrm{Re} > \mathrm{Re}^{**}$.

In [3],[5], observed vortex shedding put in correspondence with the calculated vorticity distributions $\omega(t,\mathbf{x})$. However, closed curves on the vorticity distributions in the far wake correspond to the wave motion in the far wake rather than vortex structures (Fig. 3). In accordance with [10], the observed vortex shedding put in correspondence with the $\lambda_2(t,\mathbf{x})$ boundaries of the regions of supposed existence of vortex structures in the far wake behind a sphere in [3]. However, flow patterns drawn by streamlines do not find the vortex structures within the regions of their supposed existence. In [3], the flow patterns of the near wake behind a sphere drawn by streaklines show a lines remind of horseshoe-shaped vortex loops. However, in the far wake behind a sphere, horseshoe-shaped vortex loops were not found. That is, the flow patterns drawn by streaklines also do not recorde vortex shedding. Therefore, attempts to put both vorticity distributions and boundaries of the regions of vortex structures supposed existence in correspondence to vortex shedding did not give the desired result.

It follows that calculation cannot put anything in correspondence to seven of ten experimentally observed modes schematically shown in Fig. 4. Namely, to periodic axially symmetrical pulsation of the recirculation zone not accompanied by vortex shedding $\mathbf{V}_0^{exp}(t,\mathbf{x})$, and six periodic vortex shedding modes $\mathbf{W}_0^{exp}(t,\mathbf{x})$ and $\mathbf{Q}_0^{exp}(t,\mathbf{x})$, $\mathbf{V}_1^{exp}(t,\mathbf{x})$, $\mathbf{V}_2^{exp}(t,\mathbf{x})$, $\mathbf{W}_2^{exp}(t,\mathbf{x})$, and $\mathbf{Q}_2^{exp}(t,\mathbf{x})$. Calculation determines the direction of instability development, indicated by a dashed slant line in Fig. 4. That is, after the critical Reynolds number Re^* is reached, the solutions to the Navier–Stokes equations lose the ability to predict the direction of instability developments shown in Fig. 4 by three horizontal branches. Solutions to classic hydrodynamics equations successfully reach the boundary of the unstable field shown by a dashed slant line in Fig. 4. These solutions move along the boundary of this field as Re increases. But solutions to classic hydrodynamics equations are unable to cross this boundary. In [2], the conclusion about discrepancy between the results of direct numerical integration of the Navier-Stokes equations and experiment is based on the deeper analysis. In [2], the responsibility for calculation failures has been laid on the Navier–Stokes equations themselves.

3. Transition to turbulence in shear flow

The first eigenvalue of the first front line reaches the axis ordinates at $\mathrm{Re}^{***} > \mathrm{Re}^{**}$ (Fig.2). After the passage of critical value Re^{***}, the $\mathbf{U}_2^{cal}(t,\mathbf{x})$ limiting cycle loses stability. At $\mathrm{Re} > \mathrm{Re}^{****}$, the $\mathbf{U}_2^{cal}(t,\mathbf{x})$ solution is replaced by the multiperiodic, that is, essentially chaotic, $\mathbf{U}_3^{cal}(t,\mathbf{x})$ solution. However, such scenario of turbulence appearance contradicts the experiment.

There are no experiments, in which the turbulent regime substitutes any of medium stable states, $\mathbf{U}_0^{exp}(\mathbf{x})$, $\mathbf{U}_1^{exp}(\mathbf{x})$, or $\mathbf{U}_2^{exp}(t,\mathbf{x})$. The development of each of these stable states inevitably passes through the vortex shedding mode (Fig.4). Periodic vortex shedding is an obligatory, well defined, and fairly prolonged along Reynolds number regime of transition from stability to turbulence. This is the first significant discrepancy between calculation and experiment.

The role played by fluctuations in experiments is not limited to determining the direction of turbulence development (Fig. 4). In addition, the level of medium fluctuations can substantially distort the observed flow pictures. At fairly high Re values, chaotic fluctuations grow up to the extent that we cannot see the true flow picture. Medium fluctuations are the dominant factor in determining the place of randomness emergence in regular flow picture on the Re scale.

Experiments performed in an air tunnels and experiments where body settles in medium under the action of gravitation have the highest level of fluctuations. In Fig. 4, these experiments are represented by the upper branch. In the experiment performed in [8], randomness appeared in the system at Re between Re_2^* and Re_2^{**}, Re_2^*=300, Re_2^{**}=800. Starting with Re = 420, the point of shedding began to move over the surface of the periphery of the recirculating zone, and shed vortex loops acquired irregularly twisted shapes. However, the emergence of randomness elements extremely weak distort the regular structure of vortex shedding. In the experiment performed in [9], randomness elements in vortex shedding became noticeable at Re > 700, and, in [11], randomness elements were already perceptible at Re =360.

The absence of strong chaotic fluctuations allows us to observe the regular vortex shedding without signs of randomness even at fairly high Reynolds number values. In [7], experiment was performed in water tunnel, but the principle of water circulation was not used. The level of fluctuations was likely not high, well below the fluctuation level of the air tunnel. Experiment performed in [7] recorded the regular vortex shedding over the whole range of Reynolds number values studied, up to Re = 3000. The lowest, almost thermodynamic level of fluctuations is ensured in experiments, in which the sphere is dragged horizontally through an unperturbed medium at a constant strictly controlled velocity [12], [6]. In such experiments, randomness elements are not observed on a strictly regular flow picture over the whole range of Reynolds numbers studied, up to Re = 30000 [6].

Thus, the range of emergence of randomness elements in regular flow on the Re scale to be very wide. The lower boundary of this range has a few hundreds. The upper boundary of this range has not been established. The place of emergence of randomness elements on the Re scale depends strongly on the level of medium fluctuations. This strong dependence is known since the times of O.Reynolds. The experiment records this relationship in each of the shear flows (boundary layers, jets and wakes, and flows in pipes and channels, etc.) [13].

Calculation draws a diametrically opposite picture of turbulence appearannce. The $\mathbf{U}_0^{cal}(\mathbf{x})$ basic stationary solution is markedly different from the $\mathbf{U}_1^{cal}(t,\mathbf{x})$ stationary solution (Fig. 1) and is quite different from the $\mathbf{U}_2^{cal}(t,\mathbf{x})$ limiting cycle (Fig. 3). However, as noted in Section 2, within the frameworks of linear approximation, the $\mathbf{U}_0^{cal}(\mathbf{x})$ basic stationary solution sets the direction of the flow evolution, which coincides with the direction given by the exact calculation in the range $\mathrm{Re}^* \le \mathrm{Re} \le \mathrm{Re}^{****}$. Moreover, critical values calculated in the linear approximation very poorly differ from those given by exact calculation.

It is then highly improbable that the eigenvalue field of the $\delta\tilde{\mathbf{U}}_2^{(1)cal}(t,r,z,\varphi)$ mode perturbation of the $\tilde{\mathbf{U}}_2^{cal}(t,\mathbf{x})$ solution can be qualitatively different from the eigenvalue field of the $\delta\mathbf{U}_2^{(1)cal}(t,r,z,\varphi)$ mode perturbation of the $\mathbf{U}_2^{cal}(t,\mathbf{x})$ solution if $\tilde{\mathbf{U}}_2^{cal}(t,\mathbf{x})$ differs from $\mathbf{U}_2^{cal}(t,\mathbf{x})$ only to within 0.1, which corresponds to maximum difference between the level of fluctuations in experiments performed in [8],[11] and the level of fluctuations in experiments performed in [6],[12]. Thus, a critical value of Reynolds number Re corresponding to the appearance of randomness elements at the $\mathbf{U}_2^{cal}(t,\mathbf{x})$ regular solution (according to [5], Re^{***}=300) depends very weakly or does not depend essentially on the level of fluctuations in experiment. This is the second significant discrepancy between calculation and experiment.

According to experiments, a vortex street appears in the wake behind a sphere suddenly. This occurs after the attainment of a certain critical Reynolds number value. Starting with the moment of its origination, it is fairly well defined. Unlike the regular vortex shedding, increase in randomness occurs gradually. Completely chaotic picture replaces the picture of regular vortex shedding for a large range of Reynolds number values. In experiment performed in [8], the first randomness elements appeared at Re = 420. Randomness increases as Re grows. At Re=650> Re_2^{**} (Fig. 6b), chaos may not be able to distort the regular nature of vortex shedding.

As Re increases further, the structure of vortex loops becomes less clear (Fig. 6c, Re = 1350). In Fig. 6d, the structure of vortex loops becomes obscure and increasingly difficult to distinguish from a chaotic structure. The flow pattern (Fig. 6d) recorded for the shear flow at Re = 1444. In uniform flow, the Reynolds number value corresponding to full chaotic picture will

exceed Re=1444. The reason is as follows. The flow shift should be identified with an additional increase in the level of turbulence. Thus, in accordance with experiment performed in [8], the replacement of strictly regular vortex shedding flow by completely chaotic flow occurs gradually, within the large range of Reynolds number values ($\Delta\mathrm{Re}$>1000).

Calculation draws a diametrically opposite picture of replacing the strictly regular mode by the completely chaotic mode. In accordance with Fig. 2, the distance between the first eigenvalue of the first front line and the last eigenvalue of the second front line is $\Delta\mathrm{Re}=\mathrm{Re}^{****}-\mathrm{Re}^{***}$ approximately equals 40. Apparently, the intersection of the axis of ordinates by all the eigenvalues of the first front line is the sufficient condition for high distortion of regular flow pattern, then, $\Delta\mathrm{Re}$ approximately equals 20. Further, take into account that calculated critical values in the linear approximation very poorly differ from those given by exact calculation. Thus, the regular flow pattern is replaced by a chaotic picture very quickly, within $\Delta\mathrm{Re}$ approximately equals 20. This is the third significant discrepancy between calculation and experiment.

Three significant discrepances between calculation and experiment lead to the following conclusion. The $\mathbf{U}_3^{cal}(t,\mathbf{x})$ multiperiodic, in essence, chaotic deterministic solution to classic hydrodynamics equations is not suitable for the interpretation of observed turbulence. Losing the direction of instability development, classic solutions fail into deterministic chaos, which is not directly related to the turbulence recorded experimentally.

Experiments with low level of medium fluctuations record the following set of flow regimes, replacing successively each other as Re increases: basic axially symmetric recirculating zone, pulsating recirculating zone, street of separated vortex rings, street of adjoining vortex rings, i.e., vortex sheet (the lower branch in Fig. 4). Experiments with a high level of medium fluctuations record the following sequence of flow regimes: basic axially symmetric recirculating zone, secondary non-axisymmetric recirculating zone, recirculating zone with oscillating focus, several modes of vortex shedding, turbulence (the upper branch in Fig. 4). Experiments on the flow around other bodies of simple shape (cylinder, disc, plate) record the similar sequence of modes (see review [14]).

Figure 8 demonstrates the structure of the shear layer behind a cylinder with axially symmetric paraboloidal nose at high angles of attack [15]. In experiment of [15], the body is dragged through an undisturbed medium in the air chamber. It ensures a low level of medium fluctuations. The following sequence of modes is observed: main recirculating zone (vortex) B, secondary recirculating zone S, primary recirculating zone A, street of adjoining vortex loops C, turbulence D. The secondary recirculating zone S is located between the primary and main ones. The experiment [15] records this sequence of modes in the shear layer while moving downstream along the contour of the streamlined body, accompanied by the growth of local value of Reynolds number Re. This sequence of modes is similar to one observed in the flow behind a bluff body as Re increases. In [15], titanium tetrachloride was employed to produce a dense white smoke, appearing as a result of a chemical reaction with water in the air. The vortex loop structure appears with smoke filaments in the shear layer. The visualized image records CCD camera by use a strobe flash lamps. The experiments with a fine flow visualization technique also record vortex shedding in the shear layer [16],[17],[18], and [19]. Rough flow visualization technique also records vortex structures near the surface of the streamlined body. For a long time, it is considered that the presence of these structures is necessary condition for the appearance of turbulence in laminar shear layer [13].

Fine flow visualization technique of [15] has allowed revealing the evolution of the instability in the shear layer. The experiment of [15] records two coexisting streets of vortex loops. The secondary recirculating zone S gives the origine to preceding vortex loops street. The primary recirculating zone A gives the origine to delayed vortex loops street. The preceding vortex loops appear intermittently. The delayed vortex loops are stronger in magnitude than the preceding ones. The preceding vortex loops street is difficult to observe by visualizations, since it is overshadowed by the delayed one C (Fig.8).

The process of separating the vortex loop from the recirculating zone core was studied in detail in [3] (Fig. 7). In accordance with Fig. 7, the vortex loop arises within recirculating zone. After reaching the border of the recirculating zone, vortex loop is detached from this zone and rushes downstream. Characteristic features of development of the vortex structure within the recirculating zone and type of separating vortex structure strongly depend on both the geometry of the streamlined body and the form of recirculating zone. However, it is very improbable that there is a mechanism of appearance of a vortex street different from the mechanism shown in Fig.7.

In accordance with these ideas and Figures in [15], vortex loops separate periodically from the primary recirculating zone A and rush downstream along the contour of the streamlined body. Vortex loop increases in magnitude while propagating downstream from the middle of the nose. Increasing vortex loops encircle the main recirculating zone B and extend to the cylinder part of streamlined body. The street of adjoining vortex loops (vortex sheet) has the form of wave-like folds of the shear layer C. Elements of randomness D appear at the end of nose (Fig. 8). Fine uniform vortex loops become turbulent, changing the appearance to the rough vortex loops. The process of distortion of regular flow C (Fig. 8) is similar to the process of distortion of the $\mathbf{W}_2^{exp}(t,\mathbf{x})$ regular flow (Fig. 6c).

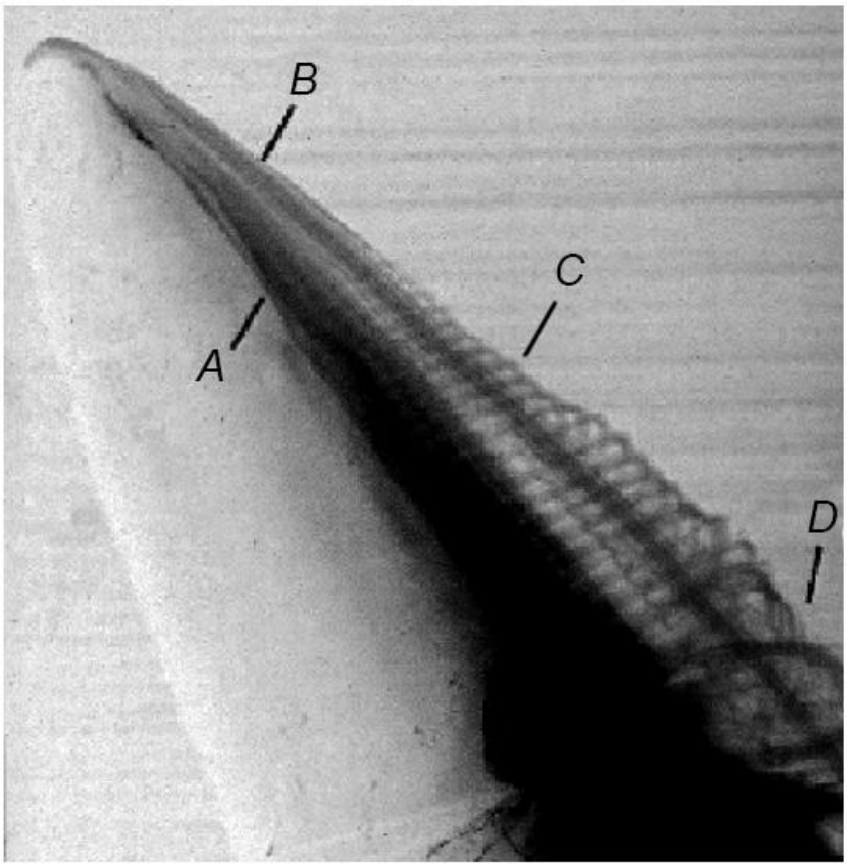

Figure 8. Shear layer behind a paraboloidal-nose cylinder: angle of attack $\alpha = 70^0$, $\mathrm{Re} = 7200$. Figure 8 was drawn using the experimental data from [15].

The established analogy between the mode sequence at instability development in the problem of flow around a sphere and the structure of shear layer behind a cylinder with the axially symmetric paraboloidal nose leads to the following conclusions. As shown in Section 2, solutions to the Navier-Stokes equations are not able to describe the process of separating the vortex loop from the recirculating zone adjacent to the surface of the streamlined body (Fig.7). As a result, solutions to these equations could not describe the phenomenon of vortex shedding represented by six regular periodic regimes in the problem of flow around a sphere. It is highly improbable that solutions to the Navier-Stokes equations can describe the process of separating the vortex loop from the recirculating zone A in more complex problem of the shear layer behind a cylinder. Therefore, it is highly improbable that solutions to the Navier-Stokes equations are able to describe the vortex loops street C (Fig.8).

Analysis of experimental data on flow around a sphere shows that the process of turbulence development strongly depends on the turbulence level in incoming flow k. The absence of strong chaotic fluctuations allows us to observe the regular flow without signs of randomness even at very high Reynolds number values (Re = 30000 in [6]). Different picture is observed at a high level of turbulence k in incoming flow (Fig. 6). The chaotic fluctuations rise strongly in the wake behind a sphere. This growth allows us to observe elements of randomness in the wake. The randomness elements grow as Re increases. Figure 6 shows that at sufficiently high values of Re, experiment records the highest level of chaotic fluctuations in the near wake, both within the core and on the periphery of recirculating zone. High level of fluctuations achieved in the near wake contributes to the spread of detached vortex loops as they move in the far wake. The structure of vortex loops becomes obscure and increasingly difficult to distinguish from the chaotic structure at sufficiently large distances from the sphere. Thus, chaotic distorting the regular flow picture by means of chaotic fluctuations growth is responsible for turbulence development (Fig. 6).

The process of turbulence development observed in Fig. 6 is correlated with the process of turbulence development in the shear layer behind a cylinder (Fig. 8). The low level of fluctuations within incoming flow k contributes to the formation of fine clearly defined vortex loops C. However, local Reynolds number value increases as we move downstream along the contour of the streamlined cylinder. Even low level of fluctuations k gives the possibility to attain the turbulent regime as local Reynolds number value increases. Namely, moving downstream from the primary recirculating zone A, each fine vortex loop spreads and gradually loses its strict contours at the end of the nose D.

In the problem of flow around a bluff body, the Navier-Stokes equations find solutions to interpret all the medium stable states, stationary and non-stationary. However, the Navier-Stokes equations do not have solutions that can interpret the phenomenon of vortex shedding. Thus, the $\mathbf{U}_3^{cal}(t,\mathbf{x})$ deterministic chaotic solution immediately follows the $\mathbf{U}_2^{cal}(t,\mathbf{x})$ limiting cycle on Re scale. That is, according to the solutions to the Navier-Stokes equations, turbulence replaces the $\mathbf{U}_2^{cal}(t,\mathbf{x})$ limiting cycle bypassing vortex shedding modes. As shown above, it is one of reasons for the insolvency of the $\mathbf{U}_3^{cal}(t,\mathbf{x})$ chaotic solution in interpretation of observed chaotic distortion of regular vortex shedding, i.e., the observed turbulence.

It is reasonable to assume that the Navier-Stokes equations also have solutions to interpret all the stable medium states (stationary and non-stationary) in the shear layer. It means that the probability of the existence of solutions to the Navier-Stokes equations, interpreting stable recirculating zone (vortices) B, S, and A in the shear layer behind a cylinder, is extremely high. However, as noted above, it is most unlikely that the Navier-Stokes equations have solutions that can be put in correspondence with the vortex shedding modes, which arise behind the vortices A and S when the flow loses stability. That is, the direct numerical integration of the Navier-Stokes equations will not be able to interpret the vortex shedding mode C in the wake behind the recirculating zone A after stability loss.

Landau scenario leads solutions, after they lose stability, to a new stable positions about which periodic motion is performed. Chaotic deterministic state is achieved as a result of sequence of Hopf bifurcations. According to Landau scenario, bifurcations inevitably lead to multiperiodic mode at the end of the body while moving downstream along the contour of the streamlined cylinder. However, solutions to the Navier-Stokes equations are also not able to pass through the vortex shedding modes during interpretation of the transition to turbulence in the shear layer. Therefore, deterministic solutions to the Navier-Stokes equations, interpreting the laminar-turbulent transition, are also not suitable to describe the observed chaotic distortion D of the vortex loops street C, that is, the observed turbulence (Fig 8).

4. Regular and chaotic components in solutions to the multimoment hydrodynamics equations.

In accordance with Section 3, experimental transition to turbulence proceeds through chaotic distortion of the regular regime of vortex shedding both in the wake behind a sphere and in the shear layer behind a cylinder. Evolution of solutions to classic hydrodynamics equations inevitably effects the attainment of deterministic chaos. However, the deterministic chaos is incapable of interpreting the experimental chaotic component of turbulence. Furthermore, as shown in Section 2, the Navier-Stokes equations are unsuitable of interpreting the experimental regular component of turbulence, that is, the vortex shedding modes. In accordance with the conclusions of [2],[14], the cause of these failures is an insufficient number of principle hydrodynamic values used in the formation of classic hydrodynamics equations.

The classic hydrodynamics equations follow directly from the Boltzmann equation and, quite naturally, involve the error inherent in the derivation of the classic kinetic equation. Namely, the two-particle distribution function in collision integral is approximated by the product of two one-particle functions. The approximation used was called the molecular chaos hypothesis («Stosszahlansatz»).The physical meaning of the Boltzmann hypothesis was disclosed in [14]. It was found that just the Boltzmann hypothesis allows classic hydrodynamics to be constructed for only three lower principal hydrodynamic values. The use of the Boltzmann hypothesis excludes higher principal hydrodynamic values from the participation in the formation of classic hydrodynamics equations.

The possibility of the improvement of classic hydrodynamics equations should be sought on the way toward an increase in the number of principal hydrodynamic values. The formalism of the method [20],[21] allows hydrodynamics equations to be derived with an arbitrary number of principal hydrodynamic values specified beforehand. In [20],[21], multimoment hydrodynamics equations are constructed using seven principal hydrodynamic values. Just these seven values are measurable moments of the one-particle distribution function.

The numerical integration of the multimoment hydrodynamics equations in the problem of flow around a solid sphere at rest [22],[23],[24],[25] showed that solutions to these equations lead the development of turbulence in the direction compatible with experiments (lower branch in Fig. 4). The stationary axisymmetric solution Sol_0 to the multimoment hydrodynamics equations satisfactorily reproduces the basic stable flow $\mathbf{U}_0^{exp}(\mathbf{x})$. Upon reaching Re_0^{*}, the solution Sol_0 loses stability. The first unstable flow $\mathbf{V}_0^{exp}(t,\mathbf{x})$ is satisfactorily described by the unstable axisymmetric solution Sol_0. Upon reaching Re_0^{**}, the unstable solution Sol_0 for the periphery of the recirculating zone and in the far wake is replaced by the non-stationary solution Sol_2, which describes a vortex ring moving downstream. The reason for the replacement is that the combination of solutions Sol_0 and Sol_2 provides a sharper drop in the entropy in the course of evolution than the solution Sol_0 does [25]. In accordance with the combination of solutions Sol_0 and Sol_2, the vortex ring separates from the core of the recirculating zone and moves downstream. The process of detachment is repeated periodically. The combination of the solutions Sol_0 and Sol_2 describes the vortex shedding mode $\mathbf{W}_0^{exp}(t,\mathbf{x})$. At $\mathrm{Re} > \mathrm{Re}_0^{***}$, the non-stationary solution Sol_2 at the periphery of the

recirculating zone and in the far wake behind the sphere is replaced by the non-stationary solution Sol_1, which also describes a vortex ring moving downstream. The reason for the replacement is that the combination of solutions Sol_0 and Sol_1 provides a sharper decrease in the entropy in the course of evolution than the combination of the solutions Sol_0 and Sol_2 does [25]. In accordance with the combination of solutions Sol_0 and Sol_1, the vortex rings periodically separate from the core of the recirculating zone and move downstream. The combination of the solutions Sol_0 and Sol_1 describes the vortex sheet $\mathbf{Q}_0^{exp}(t,\mathbf{x})$.

The multimoment hydrodynamics confirms the ideas of experiment on unstable nature of the phenomenon of vortex shedding. The intersection of the first critical Reynolds number value Re_0^* is accompanied by the stability loss. The system loses its stability when entropy produced in the system can not compensate entropy outflow through the surface confining the system. Such interpretation follows directly from the principle of retention and loss of the open system stability formulated in [25],[26]. In accordance with solutions to the multimoment hydrodynamics equations, the system, when loses its stability, remains further unstable. One unstable flow is replaced by another unstable flow as Re grows. The replacement of one unstable regime by another is governed the tendency of the system to discover the fastest path to depart from the state of statistical equilibrium. This striving follows directly from the evolution criterion formulated in [25],[26]. Thus, the evolution of solutions in any way does not follow the Landau-Hopf bifurcation scenario on the Re scale.

The multimoment hydrodynamics equations [21], as well as the classic hydrodynamics equations, govern space and time evolution of the whole ensemble of systems (Gibbs ensemble) rather than of some individual system. All the macroscopic parameters of each individual system do not equal strictly to macroscopic parameters of the statistical system. Macroscopic parameters vary within certain limits corresponding to their possible fluctuations Thus, each statistical hydrodynamic value $\bar{M}(t,\mathbf{x})$ is a linear combination of a great many dynamic hydrodynamic values. Let us denote their number by *K*, which can be infinitely large,

$$\bar{M}(t,\mathbf{x}) = \sum_{i=1}^{K} M_i(t,\mathbf{x}) \qquad K >> 1 \qquad (4.1)$$

All the dynamic hydrodynamic values $M_i(t,\mathbf{x})$ are calculated within the classic mechanics. Fluctuation $\delta M_i(t,\mathbf{x})$ at any time is defined as a difference between the dynamic and statistical hydrodynamic values,

$$M_i(t,\mathbf{x}) = \bar{M}(t,\mathbf{x}) + \delta M_i(t,\mathbf{x}) \quad i = 1,...,K, \quad K >> 1 \qquad (4.2)$$

In the regime of stability ($\mathrm{Re} < \mathrm{Re}_0^*$), the overwhelming majority of dynamic hydrodynamic values passing in the immediate vicinity of $\bar{M}(t,\mathbf{x})$ at $t = 0$ ($\delta M_i(t=0,\mathbf{x}) = M_i(t=0,\mathbf{x}) - \bar{M}(t=0,\mathbf{x}) << 1$) will remain in the vicinity of $\bar{M}(t,\mathbf{x})$ indefinitely long ($\delta M_i(t,\mathbf{x}) \sim \delta M_i(t=0,\mathbf{x})$). Statistical solution $\bar{M}(t,\mathbf{x})$ (represented by a trajectory in non-stationary case) describes most of the dynamic trajectories $M_i(t,\mathbf{x})$ with the fluctuation accuracy $\delta M_i(t,\mathbf{x}) << 1$.

The situation in the unstable range ($\mathrm{Re} > \mathrm{Re}_0^*$) is radically different. It immediately follows that each dynamic hydrodynamic value $M_i(t,\mathbf{x})$, strictly speaking, behaves in its own way. There is no unique $\bar{M}(t,\mathbf{x})$, which describes any dynamic hydrodynamic value from the set $M_i(t,\mathbf{x})$, $i = 1,...,K, \quad K >> 1$, for the whole ensemble with the fluctuation accuracy $\delta M_i(t=0,\mathbf{x}) << 1$. Initially close trajectories diverge. The Gibbs ensemble disintegrates [21],[25].

Disintegration of the Gibbs ensemble in the unstable region suggests the follows. The multimoment hydrodynamics equations governing the Gibbs ensemble as a whole are invalid in the region where solutions to these equations become unstable. Strictly speaking, to solve the unstable problem accurately, one needs to switch from the statistical to the dynamic level of description and apply the equations of classic mechanics modeling the dynamics of each individual gas particle. Another algorithm was proposed in [27]. In accordance with [27], when modeling an individual system, each statistical hydrodynamic value $\bar{M}(t,\mathbf{x})$ in the equations of conservation should be supplemented with its fluctuation component $\delta M_i(t,\mathbf{x})$ (4.2). In [22], the $\delta M_i(t,\mathbf{x})$ fluctuations are divided into two components,

$$\delta M_i(t,\mathbf{x}) = \delta M_i^R(t,\mathbf{x}) + \delta M_i^S(t,\mathbf{x}) \qquad (4.3)$$

Regular deterministic component appears in system after it loses stability. The $\delta M_i^R(t,\mathbf{x})$ regular deterministic fluctuations (4.3) are interrelated both in time and space. The regular fluctuations attain the basic order of magnitude as unstable process develops.

Stochastic (spontaneous) fluctuations $\delta M_i^S(t,\mathbf{x})$ (4.3) are random independent events. Let characteristic spatial and temporal scales be $\tilde{l}$ and $\tilde{\tau}$ correspondingly for a stochastic fluctuations. Small-scale stochastic fluctuations with $\tilde{l} << a$ and $\tilde{\tau} << \mathrm{Re}a/U_0$ contribute very little, if at all, to the distribution of the hydrodynamic values $\bar{M}(t,\mathbf{x})$. However, space and time gradients of small-scale stochastic fluctuations are of the basic order of magnitude. Small-scale stochastic fluctuations ensure fulfillment of the conservation laws in the problem of flow around a solid sphere [22],[23],[25]. The emergence of large-scale stochastic fluctuations ($\tilde{l} \sim a$ and $\tilde{\tau} \sim \mathrm{Re}a/U_0$) can introduce distortions into observed regular flow pattern. Large-scale stochastic fluctuations attain an basic order of magnitude.

Even at a relatively high flow turbulence level k, experimental chaotic fluctuations remain small-scale ones. The sharp increase in experimental chaotic fluctuations may occur in the recirculating zone after passing the critical value of Reynolds number, $\mathrm{Re} > \mathrm{Re}_0^*$. The reasons may be as follows. Figure 9 shows the time dependence of the dimensionless pair entropy $S_p^{(0)}(t)$, $S_p^{+(0)}(t^+)$ calculated from the Sol_0 unstable solution at Re=400. The details of the calculation are represented in [22],[23]. The Sol_0 unstable solution describes the $\mathbf{V}_0^{exp}(t,\mathbf{x})$ pulsations of the recirculating zone in the wake behind a sphere after the $\mathbf{U}_0^{exp}(\mathbf{x})$ solution loses stability. The intensity of pulsations increases as Re rises. Beginning from the time $t=0$ up to the time $t=t_*$, the $S_p^{(0)}(t)$ entropy decreases very sharply within the vicinity of $t=t_*$. The movement of the representative point over the $S_p^{+(0)}(t^+)$ curve from $t=t_*$ to $t=2t_*$ corresponds to the return of the recirculating zone to its original position, i.e., the position corresponding to the time $t=0$. Since the time $t=t_*$, the movement of the representative point is described by the reverse multimoment hydrodynamics equations [28]. The reverse set of equations is solved with progressive timing along the time axis. However, the positive direction of the time axis runs from the future to the past. This process is repeated with a period $T=2t_*$. At $\mathrm{Re} > \mathrm{Re}_0^*$, all the other hydrodynamic values exhibit similar behavior in the recirculating zone.

The sharp increase in the $\delta M_i^R(t,\mathbf{x})$ regular deterministic fluctuations within the recirculating zone is balanced by sharp rise in the $\delta M_i^S(t,\mathbf{x})$ stochastic fluctuations in the conservation equations [22],[23],[25]. It is likely that there are many options for balancing. However, large-scale stochastic fluctuations are more preferred in this process compared to the small-scale stochastic fluctuations. Indeed, the emergence of large-scale stochastic fluctuations corresponds to a stronger deviation of system state from the state of statistical equilibrium, i.e., to a lower entropy. Therefore, the instability development through the development of large-scale stochastic fluctuations provides a faster path to depart from the state of statistical equilibrium compared to instability development through the development of small-scale stochastic fluctuations. Then, in accordance with the evolution criterion [25],[26], the system will go along the instability development path contained large-scale stochastic fluctuations. Moreover, before large-scale fluctuations arrive at the periphery of recirculating zone at the instant of separation, they may experience some periods of sharp increase in the recirculating zone (Fig. 9), i.e., to increase many times over.

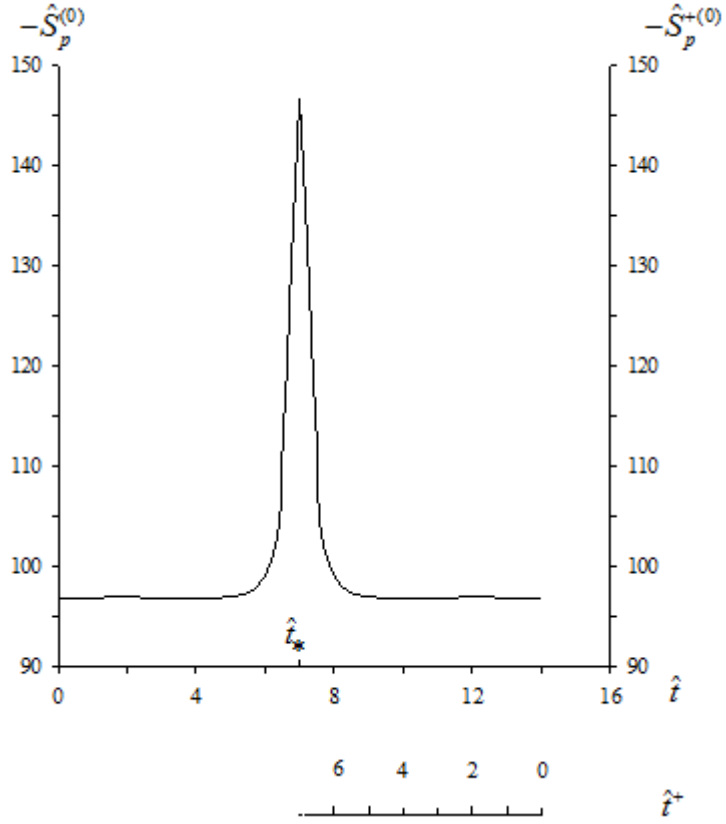

Figure 9. Time behavior of the pair entropy $\hat{S}_p^{(0)}(t)$, $\hat{S}_p^{+(0)}(t^+)$, $\mathrm{Re}=400$, $\hat{t}_* = 6.99$.

5. Conclusions

Experiment records three stable medium states for flow past a sphere. The $\mathbf{U}_0^{exp}(\mathbf{x})$ stable stationary flow consists of an axisymmetric toroidal recirculating zone in the near wake (Fig. 1), which originates a single rectilinear thread in the far wake. The $\mathbf{U}_1^{exp}(\mathbf{x})$ stable non-axisymmetric flow consists of two weakly asymmetric halves in the near wake, which originate two rectilinear threads in the far wake. The $\mathbf{U}_2^{exp}(t,\mathbf{x})$ central-type stable state is characterized by periodic restructuring in the near non-axisymmetric wake, which causes wavy motion in the far wake (Fig. 3).

Each of the three stable states, $\mathbf{U}_0^{exp}(\mathbf{x})$, $\mathbf{U}_1^{exp}(\mathbf{x})$, and $\mathbf{U}_2^{exp}(t,\mathbf{x})$, is characterized by its own direction of turbulence development different from the other directions. These directions are schematically shown by three horizontal branches in Fig. 4. Turbulence begins to develop upon the attainment of critical Reynolds number values, $\mathrm{Re}_0^*, \mathrm{Re}_1^*$, and Re_2^*, respectively. Turbulence development inevitably involves periodic vortex shedding modes. Each of the three turbulence development directions has vortex shedding features of its own only characteristic of the given direction. No matter what direction is selected by experiments, periodic vortex shedding is, however, an unavoidable, well-defined turbulence-development mode, which is fairly extended along the Re scale. Experiment records six vortex shedding modes $\mathbf{W}_0^{exp}(t,\mathbf{x})$, $\mathbf{Q}_0^{exp}(t,\mathbf{x})$, $\mathbf{V}_1^{exp}(t,\mathbf{x})$, $\mathbf{V}_2^{exp}(t,\mathbf{x})$, $\mathbf{W}_2^{exp}(t,\mathbf{x})$, and $\mathbf{Q}_2^{exp}(t,\mathbf{x})$, and one pulsation mode $\mathbf{V}_0^{exp}(t,\mathbf{x})$. The recorded set of regular unstable periodic modes is most likely incomplete.

The direct numerical integration of the Navier-Stokes equations in the problem of flow around a solid sphere at rest was performed in [3],[5]. In this problem with time independent boundary conditions calculation finds two stable stationary solutions, $\mathbf{U}_0^{cal}(\mathbf{x})$ and $\mathbf{U}_1^{cal}(\mathbf{x})$, and the $\mathbf{U}_2^{cal}(t,\mathbf{x})$ stable non-stationary limiting cycle. Apart from the $\mathbf{U}_0^{cal}(\mathbf{x})$, $\mathbf{U}_1^{cal}(\mathbf{x})$, and $\mathbf{U}_2^{cal}(t,\mathbf{x})$ solutions, the Navier-Stokes equations only have multiperiodic, that is, essentially chaotic, solution $\mathbf{U}_3^{cal}(t,\mathbf{x})$. The numerical integration of the Navier-Stokes equations shows that turbulence development occurs in strict correspondence to the Landau-Hopf scenario [1]. Accordingly, after some critical Reynolds number value Re^* is reached, the $\mathbf{U}_0^{cal}(\mathbf{x})$ solution loses

stability and experiences bifurcation to the $\mathbf{U}_1^{cal}(\mathbf{x})$ solution (regular bifurcation). The $\mathbf{U}_1^{cal}(\mathbf{x})$ solution, after it loses stability at $\mathrm{Re}^{**} > \mathrm{Re}^{*}$, experiences bifurcation to the $\mathbf{U}_2^{cal}(t,\mathbf{x})$ limiting cycle (the Hopf bifurcation). After some Reynolds number value Re^{***} is reached, the $\mathbf{U}_2^{cal}(t,\mathbf{x})$ limiting cycle loses stability and is substituted by the $\mathbf{U}_3^{cal}(t,\mathbf{x})$ deterministic chaotic solution. It follows that, according to Landau-Hopf scenario, the system, after it loses stability, inevitably reaches a new stable position and experiences either periodic or chaotic motion about it. Calculation determines the direction of instability development, indicated by a dashed slant line in Fig. 4.

According to the modeling performed in [3],[5], the evolution of the $\mathbf{U}_0^{cal}(\mathbf{x})$ solution follows the slant direction (Fig. 4), whereas experiment directs the evolution of $\mathbf{U}_0^{exp}(\mathbf{x})$ in the horizontal direction along the lower branch. According to [3],[5], the evolution of $\mathbf{U}_1^{cal}(\mathbf{x})$ occurs in the slant direction (Fig. 4), whereas experiment directs the evolution of $\mathbf{U}_1^{exp}(\mathbf{x})$ in the horizontal direction along the middle branch. According to [5], the $\mathbf{U}_2^{cal}(t,\mathbf{x})$ solution loses stability to be replaced by the $\mathbf{U}_3^{cal}(t,\mathbf{x})$ chaotic solution, whereas experiment directs the evolution of $\mathbf{U}_2^{exp}(t,\mathbf{x})$ along the upper branch shown in Fig. 4. It follows that calculations give turbulence development direction incompatible with experiment.

The separation of the shed vortex loop from the recirculating zone is very clearly shown in Fig. 7. Figure 7 gives the idea of the vortex shedding phenomenon. The experimental vortex structure engendered begins to expand and moves downstream within the recirculating zone. After reaching the periphery of the recirculating zone, this vortex structure separates from this zone and rushes downstream. An attempt to put the $\mathbf{U}_2^{cal}(t,\mathbf{x})$ limiting process in correspondence with the observed $\mathbf{V}_2^{exp}(t,\mathbf{x})$ vortex shedding did not give the desired result. The $\mathbf{U}_2^{cal}(t,\mathbf{x})$ limiting cycle is incapable of reproducing the $\mathbf{V}_2^{exp}(t,\mathbf{x})$ vortex shedding mode (Fig. 3). Really, after the appearance in the upper half of the wake behind a sphere, the size of the vortex structure becomes substantial at the surface of the sphere. Subsequently, the structure moves toward the periphery of the recirculating zone, which is accompanied by its continuous dissipation. Lastly, it fully disappears at the periphery of the recirculating zone. This is an essential difference between calculation and experiment. Because of the absence of the detachment of the recirculating zone periphery in Fig. 3, there is no vortex loop street in the far wake behind a sphere.

Thus, the $\mathbf{U}_0^{cal}(\mathbf{x})$, $\mathbf{U}_1^{cal}(\mathbf{x})$, and $\mathbf{U}_2^{cal}(t,\mathbf{x})$ solutions satisfactorily reproduce three stable flows observed experimentally, $\mathbf{U}_0^{exp}(\mathbf{x})$, $\mathbf{U}_1^{exp}(\mathbf{x})$, and $\mathbf{U}_2^{exp}(t,\mathbf{x})$. However, calculation are incapable of reproducing any of six periodic vortex shedding modes observed along the three turbulence development directions (Fig. 4). Moreover, after the critical Reynolds number Re^{*} is reached, the Navier-Stokes equations lose the ability to predict the directions of turbulence development shown in Fig. 4 by three horizontal branches.

Losing direction of instability development, classic hydrodynamics equations arrive at deterministic, multiperiodic, in essence, chaotic solution $\mathbf{U}_3^{cal}(t,\mathbf{x})$. The study of possibility to use the $\mathbf{U}_3^{cal}(t,\mathbf{x})$ solution of interpreting the observed appearance and development of turbulence has revealed three significant discrepancies. Firstly, the development of each of the stable medium states $\mathbf{U}_0^{exp}(\mathbf{x})$, $\mathbf{U}_1^{exp}(\mathbf{x})$, and $\mathbf{U}_2^{exp}(t,\mathbf{x})$, inevitably passes through the vortex shedding mode (Fig. 4). There are no experiments, in which the turbulent regime replaces any of these stable states bypassing vortex shedding modes. On the contrary, calculated transition to turbulence bypasses the modes of vortex shedding.

Secondly, the level of medium fluctuations (disturbances) is the dominant factor in determining the place of randomness appearance in regular flow pattern on the Re scale. Experiment records the first manifestations of the randomness in the regular flow within a very wide range of Reynolds number values. The lower boundary of this range equals to a few hundreds. The upper boundary has not been established. In experiment with low level of fluctuations [6], randomness was not observed in a strictly regular flow pattern over the whole range of Reynolds numbers studied, up to Re = 30000. Calculation draws a diametrically opposite picture of turbulence onset. The critical value of Reynolds number Re^{***}, which corresponds to origin of randomness in regular solution, depends very weakly or, in essence, does not depend at all on the experimental level of fluctuations (Re^{***} =300 was reported in [5]).

Thirdly, according to experiment, completely chaotic picture substitutes the strictly regular vortex shedding pattern gradually, over a wide range of Reynolds number values ($\Delta\mathrm{Re}$>1000). Calculation draws a diametrically opposite picture for such substitution. Namely, highly chaotic picture replaces strictly regular flow pattern very quickly, within $\Delta\mathrm{Re}$ approximately equals 20.

The analogy is revealed between the sequence of modes at instability development in the problem of flow around a sphere and the structure of the shear layer behind axisymmetric cylinder with paraboloidal nose. Namely, the sequence of modes observed in the flow around a sphere as Re increases (Fig. 4) is similar to the sequence of modes recorded while moving downstream

along the contour of the streamlined cylinder (Fig. 8). Figure 8 demonstrates two recirculating zones (vortexes) A and B, street of vortex loops C, turbulence D. Vortex loops periodically separate from the recirculating zone A and rush downstream. The street of adjoining vortex loops (vortex sheet) has the form of wave-like folds of the shear layer C. At the end of the nose D, vortex loop loses its strict contours. Characteristic features for the development of vortex structure within recirculating zone and type of separating vortex structure strongly depend on both the geometry of the streamlined body and the form of recirculating zone. However, it is highly improbable that there is a mechanism of vortex street occurrence different from the mechanism shown in Fig. 7. Namely, vortex loop engendered within the recirculating zone separates from it and rushes downstream.

Figure 8 is obtained through a fine flow visualization technique in the experiment [15]. However, a great number of experiments, fine and coarse, records stable vortexes and vortex streets in the shear layer at a surface of streamlined profile. Therefore, it is reasonable to assume that the mechanism of transition to turbulence in the shear layer behind cylinder with the axisymmetric paraboloidal nose recorded in [15] is common (probably the only one) for each of shear layers.

Experimental studies have shown that the mechanisms for turbulence development in boundary layers and channels are universal [29],[30]. Therefore, it is expected that the scenario of transition to turbulence as a result of chaotic distortions of regular unstable medium state is suitable for the interpretation of the laminar-turbulent transition in channels and pipes.

Analysis of experimental data shows that the turbulence in shear flow is the result of chaotic distortion of regular vortex shedding regime. That is, the turbulence of shear flow is the vortex shedding regime distorted by chaotic fluctuations. The vortex shedding is the regular component of turbulence. In the turbulent flow, each hydrodynamic value is a linear combination of regular and chaotic components. More precise definition is as follows. The turbulence of shear flow is regular unstable regime distorted by chaotic fluctuations. This elaboration greatly supplements turbulent picture. Indeed, the $\mathbf{V}_0^{exp}(t,\mathbf{x})$ regular unstable mode also takes part in development of turbulence. Moreover, the sharp rise in the chaotic fluctuations, which distort the regular unstable flow, is simulated by sharp increase in the hydrodynamic values within the recirculating zone at the $\mathbf{V}_0^{exp}(t,\mathbf{x})$ pulsating mode.

In the problem of flow around a sphere, solutions to the Navier-Stokes equations satisfactorily reproduce all the observed stable flows. However, the Navier-Stokes equations do not possess the solutions to interpret the process of vortex structure separation from the core of recirculating zone, i.e., the vortex shedding. Thus, the Navier-Stokes equations are not able to interpret the regular component of turbulence. It is reasonable to assume that the Navier-Stokes equations also have the solutions to interpret all stable medium states, stationary and non-stationary, in shear layer. This means that the Hopf bifurcations consistently lead to stable solutions, which interpret recirculating zones (vortices) A and B in the shear layer behind a cylinder (Fig. 8). However, it is highly improbable that these stable solutions will be able to describe the process of vortex loop separation from recirculating zone in more complex problem of the shear layer behind a cylinder. That is, it is extremely unlikely that stable non-stationary solutions to the Navier-Stokes equations may be put in correspondence with the vortex shedding C in the shear layer. According to Landau scenario, a sequence of Hopf bifurcations will inevitably lead the solutions to classic hydrodynamics equations to a chaotic deterministic solution while moving downstream along the contour of streamlined body in the shear layer.

In problem of flow around a sphere, the loss of direction of instability development is completed by attainment of the $\mathbf{U}_3^{cal}(t,\mathbf{x})$ deterministic chaotic solution. The $\mathbf{U}_3^{cal}(t,\mathbf{x})$ deterministic solution is not able to interpret the observed chaotic distortion of the vortex streets, $\mathbf{V}_2^{exp}(t,\mathbf{x})$ and $\mathbf{W}_2^{exp}(t,\mathbf{x})$ (Fig. 6). That is, the deterministic chaotic solution to the Navier-Stokes equations is not able to describe the chaotic component of turbulence.

During the interpretation of the transition to turbulence in the shear layer behind a cylinder, solutions to the Navier-Stokes equations also can not take into consideration the vortex shedding modes. Therefore, it is reasonable to assume that the deterministic solutions to the Navier-Stokes equations, interpreting the laminar-turbulent transition, are not suitable to describe the observed chaotic distortion D of the vortex loops street C, that is, the observed turbulence (Fig. 8). Thus, the deterministic chaos is a dead end, into which solutions to the Navier-Stokes equations fail as a result of movement in the wrong direction.

References

1. Schuster HG. Deterministic Chaos. Weinheim: Physik Verlag; 1984.

2. Lebed IV, Umanskii SY. The appearance and development of turbulence in a flow past a sphere: problems and the existing approaches to their solution. Russian Journal of Physical Chemistry B 2007; 1: 52-73. http://dx.doi.org/10.1134/S1990793107010071

3. Johnson TA, Patel VC. Flow past a sphere up to a Reynolds number of 300. Journal of Fluid Mechanics 1999; 378: 19-70. http://dx.doi.org/10.1017/S0022112098003206

4. Natarajan R, Acrivos A. The instability of the steady flow past spheres and disks. Journal of Fluid Mechanics 1993; 254: 323-344. http://dx.doi.org/10.1017/S0022112098003206

5. Tomboulides AG, Orszag SA. Numerical investigation of transitional and weak turbulent flow past a sphere. Journal of Fluid Mechanics 2000; 416:45-73. http://dx.doi.org/10.1017/S0022112000008880

6. Chomaz JM, Bonneton P, Hopfinger EJ. The structure of the near wake of a sphere moving horizontally in a stratified fluid. Journal of Fluid Mechanics 1993; 234: 1-21. http://dx.doi.org/10.1017/S0022112093002009

7. Achenbach E. Vortex shedding from spheres. Journal of Fluid Mechanics 1974; 62: 209-221. http://dx.doi.org/10.1017/S0022112074000644

8. Sakamoto H, Haniu H. The formation mechanism and shedding frequency of vortices from a sphere in uniform shear flow. Journal of Fluid Mechanics 1995; 287: 151-171. http://dx.doi.org/10.1017/S0022112095000905

9. Magarvey RH, Bishop RL. Transition ranges for three-dimensional wakes. Canadian Journal of Physics 1961; 39: 1418-1422. http://dx.doi.org/10.1139/p61-169

10. Jeong J, Hussain F. On the identification of a vortex. Journal of Fluid Mechanics 1995; 285: 69-94. http://dx.doi.org/10.1017/S0022112095000462

11. Ormieres D, Provansal M. Transition to turbulence in the wake of a sphere. Physical Review Letters 1999; 83: 80-83.

12. Taneda S. Experimental investigation of the wake behind a sphere at low Reynolds numbers. Journal of the Physical Society of Japan 1956; 11: 1104-1108. http://dx.doi.org/10.1143/JPSJ.11.1104

13. Loitsyanskii LG. Mechanics of Liquids and Gases. Oxford: Pergamon; 1966.

14. Lebed IV. About the prospects for passage to instability. Open Journal of Fluid Dynamics 2013; 3: 214-229. http://dx.doi.org/10.4236/ojfd.2013.33027

15. Mikami F., Toyota R., Nishikawa N. Observation of the instability of the shear layer behind a paraboloidal-nose cylinder. Journal of Physics, Conference Series 2010; 216: 012013. http://dx.doi.org/10.1088/1742-6596/216/1/012013

16. Riley AJ, Lowson MV. Development of a three-dimensional free shear layer. Journal of Fluid Mechanics 1998; 369: 49-89.

17 Kohama Y, Onodera T, Egami Y. Design and control of crossflow instability field. Nonlinear Instability and Transition in Three-Dimensional Boundary Layers. Ed. By P.W.Duck, P.Hall: Fluid Mechanics and its Application. Dordrecht: Kluver; 1996, 147-156.

18. Acarlar MS, Smith CR. A study of hairpin vortices in a laminar boundary layer. Part1. Hairpin vortices generated by fluid injection. Journal of Fluid Mechanics 1987; 175: 1-41. http://dx.doi.org/10.1017/S0022112087000272

19. Acarlar MS, Smith CR. A study of hairpin vortices in a laminar boundary layer. Part2. Hairpin vortices generated by a hemisphere protuberance. Journal of Fluid Mechanics 1987; 175: 43-83. http://dx.doi.org/10.1017/S0022112087000284

20. Lebed IV. Derivation of the equations for pair distribution functions. Chemical Physics Reports 1995; 14: 599-615.

21. Lebed IV. Method of two-particle distribution functions. Hydrodynamic equations. Chemical Physics Reports 1996; 15: 861-883.

22. Lebed IV. The method of pair functions as applied to the problem of a flow around a quiescent solid sphere. Chemical Physics Reports 1997; 16: 1263-1301.

23. Lebed IV. About the behavior of the entropy of a gas flow losing its stability. Chemical Physics Reports 1998; 17: 411-439.

24. Lebed IV. Development of instability in the problem of flow around a sphere. Russian Journal of Physical Chemistry B 2014; 8: 240-253. http://dx.doi.org/10.1134/S1990793114020171

25. Lebed IV. Multimoment hydrodynamics in problem on flow around a sphere: entropy interpretation of the appearance and development of instability. Open Journal of Fluid Dynamics 2014; 4: 163-206. http://dx.doi.org/10.4236/ojfd.2014.42015

26. Lebed IV. Evolution of unstable system. Journal of Advances in Physics 2015; 9: 2487-2502.

27. Lifshitz EM, Pitaevskii LP. Course of Theoretical Physics, Vol. 9: Statistical Physics, Part 2 New York: Pergamon; 1980.

28. Lebed IV. About appearance of the irreversibility. Open Journal of Fluid Dynamics 2014; 4: 298-320. http://dx.doi.org/10.4236/ojfd.2014.43023

29. Elofsson PA, Alfredsson PH. An experimental investigation of oblique transition in plain Poiseuille flow. Journal of Fluid Mechanics 1998; 358: 177-202. http://dx.doi.org/10.1017/S0022112097008288

30. Elofsson PA, Alfredsson PH. An experimental investigation of oblique transition in a Blasius boundary layer flow. European Journal of Mechanics B/Fluids 2000; 19: 615-636.